ECN
Energy research Centre of the Netherlands

# IEA Annex XX: Dynamic Inflow effects at fast pitching steps on a wind turbine placed in the NASA-Ames wind tunnel

**J.G. Schepers**

ECN-E--07-085

## Acknowledgement

'Financial support for this research was given in part by Senter-Novem, Project: 'IEA Annex XX: Analysis of NASA-Ames wind tunnel measurements' Project Reference: 2020-02-11-10-005. ECN project number: 74189.

This project could not be performed without the supply of data by the National Renewable Energy Laboratory, NREL in the USA, where in particular the support from Scott Schreck is highly appreciated.

## Abstract

This report describes a study on dynamic inflow effects which is carried out within the framework IEA Annex XX 'Analysis of NASA-Ames wind tunnel measurements'. The study makes use of measurements which were taken by NREL on a wind turbine which was placed in the large (24.4x36.6m) NASA-Ames wind tunnel.

# Contents

## Summary

This report describes a study on Dynamic Inflow effects which is performed within IEA Annex XX 'Analysis of NASA-Ames wind tunnel measurements'. The study makes use of measurements at fast (upward and downward) pitching steps on a 2-bladed wind turbine with a diameter of 10 m, which was placed in the large (24.4x36.6m) NASA-Ames wind tunnel. These measurements were carried out in Spring 2000 by the National Renewable Energy Laboratory NREL in the USA. One of the wind turbine blades was instrumented with pressure taps at 5 radial positions. The resulting pressure distributions at these 5 positions have been integrated to sectional loads. The measurements have been processed in a way that makes them suitable for comparison with calculational results from the aero-elastic code PHATAS and from the free wake lifting line code AWSM. The most important conclusions from the study are:

- The present measurements showed clear dynamic inflow effects, in particular at the upward pitching step. The dynamic inflow effects caused a large load overshoot which is followed by a gradual approach of the new equilibrium approach.
- The measurements allowed an assessment of the radial dependancy on the dynamic inflow effect.
- The agreement between the measured blade normal forces and the results obtained from the PHATAS code was good;
- The agreement between the measured blade normal forces and the calculational results from the AWSM code was even excellent in terms of:
  - Equilibrium values of normal forces;
  - Overshoots in normal forces in reaction to the step in blade pitch angle
  - Time constants. These characterize the gradual approach of the normal forces towards the equilibrium values after the overshoot.
- The time constant in the measured and AWSM results, hardly reduces towards the tip. This is opposite to the results and theoretical expectations from earlier projects and from the engineering model for dynamic inflow as implemented in PHATAS.

## notations

| | | |
|---|---|---|
| a | Axial induction factor (=$u_i/V_w$) | - |
| B | Number of blades | - |
| $C_P$ | Power coefficient | - |
| $C_{D.ax}$ | Axial force coefficient | - |
| c | chord | m |
| $c_d$ | Profile drag coefficient | - |
| $c_l$ | Profile lift coefficient | - |
| $c_n$ | Normal force coefficient | - |
| $F_{ax}$ | Axial force | N |
| $f_{cl}$ | Factor in 3D correction for lift coefficient | - |
| $f_a$ | Factor in dynamic equation for induced velocity | - |
| f | Time scale | s |
| n | Normal force (normal to the chord) per unit length | N/m |
| $M_{flat}$ | Flatwise moment (perpendicular to tip chord) | Nm |
| $M_{torq}$ | Rotorshaft torque | Nm |
| R | Rotor radius | m |
| r | Radial position relative to rotor centre | m |
| rpm | Rotor speed | [rpm] |
| t | Time | [s] |
| $u_i$ | Axial induced velocity | [m/s] |
| $V_{eff}$ | Wind speed at blade element | (m/s) |
| $V_{tun}$ | Tunnel speed | (m/s) |
| $V_w$ or $V_{wind}$ | Wind speed | (m/s) |
| $\alpha$ | Angle of attack | deg |
| $\Gamma$ | Vortex strength | $m^2/s$ |
| $\gamma$ | Vorticity density | m/s |
| $\lambda$ | Tip speed ratio ($\Omega R/V_w$) | - |
| $\phi_r$ or $\phi$ | Azimuth angle | deg |
| $\Omega$ | Rotor speed | [rpm] |
| $\rho$ | Air density | [$kg/m^3$] |
| $\sigma$ | local solidity ($Bc/2\pi r$) | deg |
| $\theta$ | Pitch angle (positive towards smaller angle of attack) | deg |
| $\tau$ | Time constant | s |

Subscripts

| | |
|---|---|
| 1 | First equilibrium value |
| 2 | Second equilibrium value |
| 2D | Two dimensional value |
| 3D | Three dimensional value |
| t | tangential |

# 1 Introduction

Wind turbines operate in a very instationary environment. Nevertheless wind turbine design codes commonly rely on the quasi-stationary blade element momentum (bem) theory. One of the limitations in this theory is the assumption of an equilibrium wake situation which is not valid for situations where a sudden change in pitch angle, rotor speed or wind speed occurs. In such cases the wake behind the turbine, and consequently the induction and the resulting effective velocity in the rotor plane will achieve steady state conditions after a certain delay. This phenomenon is commonly called 'dynamic inflow' (Alternatively, the names 'dynamic wake' or 'dynamic induction' are sometimes used). It was studied extensively in two European 'Dynamic Inflow' projects, see [5] and [8]. In these European 'Dynamic Inflow projects' several models have been developed and implemented in design codes. The models have been validated with measurements at fast pitching steps which were performed by the Danish University of Technology on the 60 m diameter Tjæreborg turbine. The pitching steps led to clear overshoots in the rotorshaft torque and the blade root flatwise moment. These load overschoots were shown to be a result of the above mentioned delay in induction.

The dynamic inflow effects have a large practical importance, not only in view of the higher dynamic loads on a turbine but also because of its impact on the aerodynamic damping characteristics and in particular in the design of pitch control algorithms, see [11].

The measurements from the European Dynamic Inflow projects offered unique insights since they gave experimental evidence of dynamic inflow effects. Nevertheless the validation did suffer from a few shortcomings. Among others the field environment and the associated instationary, unknown and uncontrollable conditions gave uncertainties. Although this problem was partly overcome by averageing over a large number of measurement campaigns, some fluctuations from the field conditions remained in the averaged time series (partly because of the structural dynamic effects). These fluctuations interfere with the fluctuations from the 'pure' dynamic inflow effect.

Another, even more important, problem is the fact that the rotor shaft torque and the blade root flatwise moments 'hide' the dependency of the aerodynamic loads on the local radius, since they are a result of the integration of the load distribution along the entire blade span. This is a major drawback in the validation since the radial dependency of the dynamic inflow effect is expected to be very strong.

The measurements which are used in the present study, are performed by the National Renewable Energy Laboratory (NREL) on a 10 m diameter wind turbine which was placed in the large 24x36.5 m wind tunnel of NASA-Ames. Again measurements have been taken at fast pitching steps. One of the wind turbine blades was instrumented with pressure taps at 5 radial position. The resulting pressure distributions at these 5 positions have been integrated to sectional loads. As such these measurements do offer the radial dependency of dynamic inflow with an additional advantage of being taken in controllable and well defined wind tunnel conditions.

The present report is structured as follows:

In section 2 a short description is given of the dynamic inflow phenomenon. It is mainly based on the findings from the European Dynamic Inflow projects. In section 3 the NASA-Ames wind tunnel measurements at fast pitching steps are described. Next, in section 4 two methods are reported which are available at ECN to model dynamic inflow. The first model has been developed in the European Dynamic Inflow projects and is of an engineering type. The qualification 'engineering' is meant to indicate that the model is easily included in industrial design codes without unduly increasing computational time. The second model is based on a much more physical representation of the wake by means of a free vortex wake method. Next, the analysis of the measurements is reported in section 5. The analysis among others takes place by comparing the measurements with the modelling results. In section 6 the influence of dynamic stall and structural dynamics on the results is investigated. Finally, section 7 quantifies the time constant which is a characteristic

parameter of the dynamic inflow process.

# 2 Dynamic Inflow: Physical phenomenon and practical consequences

In an equilibrium situation, the axial flow velocity (inflow) in the rotor plane depends on the wind speed and on the degree of loading (axial force) of the turbine. For instance, for a turbine with zero loading (Figure 1, at the top), the wind speed in the rotor plane is equal to the free stream wind speed, while an operating, loaded wind turbine slows down the wind speed to a lower value, (Figure 1, at the bottom).

The difference between (the axial component of) the wind speed and the axial flow velocity in the rotor plane is usually called the 'induced' velocity $u_i$, i.e. the axial velocity component induced by the presence of the turbine. In the actual operation of the wind turbine, its load situation is changing continuously, either because of wind speed fluctuations or through blade angle variations or rotor speed variations. Nevertheless, most of the operational computer codes for the prediction of these loads and of the dynamic behaviour of turbines, rely on the blade element momentum theory. This theory is computationally efficient but it is basically of a quasi-steady character. Hence at any instant in time, the induced velocity follows the load situation instantaneously. However when the loading situation changes, the induced velocity will lag behind, since an appreciable amount of air must be accelerated or decelerated. Therefore, differences may occur which can be attributed to unsteadiness and the time lag in the adjustment in the induced velocity during pitching, rotor speed or wind speed transients.

The phenomenon can more conveniently be explained in terms of a vorticity representation of the wake (and the blades). The wake vorticity exists of shed vorticity and trailing vorticity, both time dependent. Dynamic inflow phenomena depend mainly on the trailing vorticity (i.e. the vorticity related to the spanwise variation of the bound vortex), where the shed 'vorticity' (i.e. the vorticity related to the unsteady variation of the bound vortex) is accounted for through unsteady profile aerodynamics. The trailed vorticity is formed at the blade and convected downstream with the local total velocity, partly wake induced, see Figure 2.

Then a change in bound vorticity (e.g. through a change in pitch angle) modifies the vorticity which is trailed into the wake. Due to the fact that the vorticity is convected with a finite velocity, the resulting wake becomes a mixture of 'old' and 'new' vorticity. Consequently the velocity induced by such wake includes a contribution from the 'old' and the 'new' situation. As soon as the 'old' vorticity has 'travelled' a distance of some 2 to 4 diameters behind the rotor, its influence is hardly 'felt' anymore in the rotorplane and the new equilibrium situation is reached. However, before the vorticity has travelled this distance, a gradual change of the induced velocity takes place from its old equilibrium value to its new equilibrium value. It is this gradual change in induced velocity which is the essential characteristic of the dynamic inflow phenomenon.

In the aforementioned European Dynamic Inflow projects the phenomenon has been investigated in detail and engineering models were developed which include the most important dynamic wake effects. The characterisation 'engineering model' is meant to say that they can be implemented in industrial design codes with only a limited increase in computational effort. Thereto the models were relatively slight modifications to the standard BEM theory. The models have been validated with measurements. For this purpose the response of rotorshaft torque and flatwise moments at full span pitching steps on the Danish Tjæreborg turbine (D=60 m, constant speed) have been measured by the Danish Technical University, DTU. In these transients, after an initial period, the blade pitch angle is first increased at a fast rate, next maintained constant for some period and then decreased to its initial value at a fast rate.

Some typical results are shown in Figures 3 and 4. Figure 3 shows (qualitatively) the time series for a step on the pitch angle together with the calculated response of the induced velocity. The induced velocities are calculated from a conventional equilibrium blade element momentum theory and from ECN's engineering model for dynamic inflow which is described in [5] and in section 4. The equilibrium BEM model gives an instantaneous response of the induced velocity

where the dynamic inflow model shows the above mentioned gradual behaviour in which the new equilibrium value is reached only after a certain period.

Figure 4 shows the response of the calculated and measured rotorshaft torque. In order to reduce the influence of turbulence, wind shear and tower shadow in the measured response, DTU synchronised nine time series with respect to the pitch angle change. These nine time series were averaged. The calculated results in Figure 4 are again obtained from ECN's dynamic inflow model and from a conventional equilibrium wake model.

Figure 4 clearly shows the improved prediction from the dynamic inflow model: A large overshoot in torque is visible after the step on the pitch angle which is not predicted at all with the conventional momentum theory. The load overshoot is a result of the lag in induced velocity. This can be understood by considering two effects (illustrated for the downward pitching step):

1 The first effect is a sudden increase in angle of attack due to the pitching motion of the blade itself. This leads to an almost instantaneous increase of the torque (the delay coming from instationary airfoil aerodynamics, of which shed vorticity is an important component, and which has a very short time scale (in the order of $c/\Omega r$) );

2 The second effect is the response of the rotorshaft torque to the induced velocity. In the new equilibrium situation, the induced velocity is larger (Figure 3) and the axial wind speed through the rotor plane is lower. This reduces the rotorshaft torque, by which the increase in rotorshaft torque from effect 1 is partly compensated. As a result, the overall increase in rotorshaft torque turns out to be very limited in the new equilibrium situation (Figure 4).

However the compensating second effect only comes into play after a certain period in time, since the lag in induced velocity from Figure 3 takes place with a time scale in the order of D/U (see section 4.1). This time scale is much longer than the time scale from the instationary airfoil aerodynamics ($c/\Omega r$). Hence the rotorshaft torque will initially be determined by effect 1, causing a temporary enlargement of the rotorshaft torque. Thereafter the gradual increase of the induced velocity reduces the rotorshaft torque.

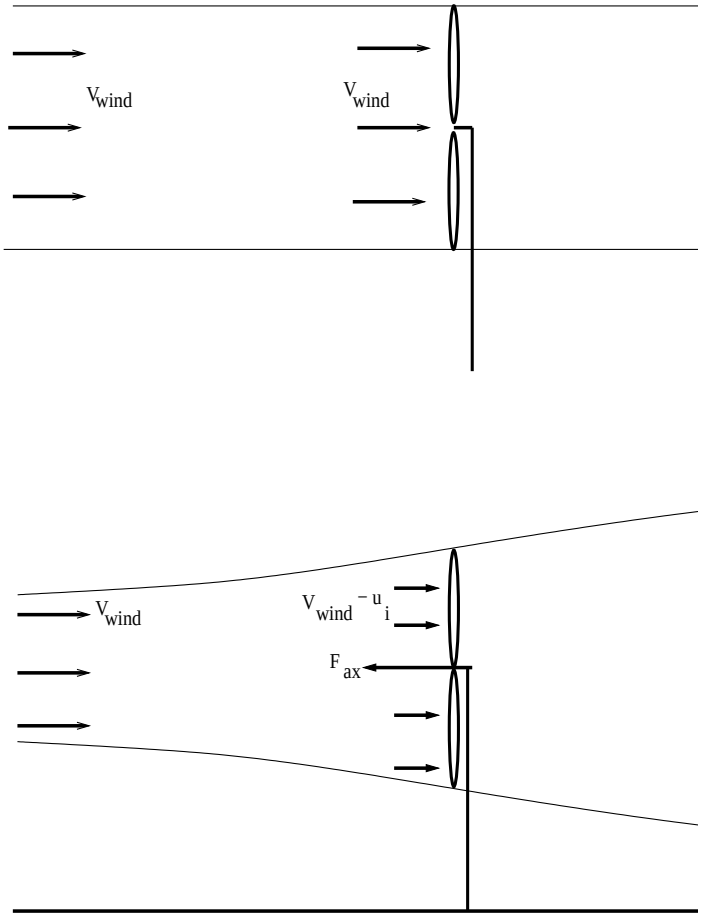


Figure 1: Streamtube with loaded and unloaded turbine

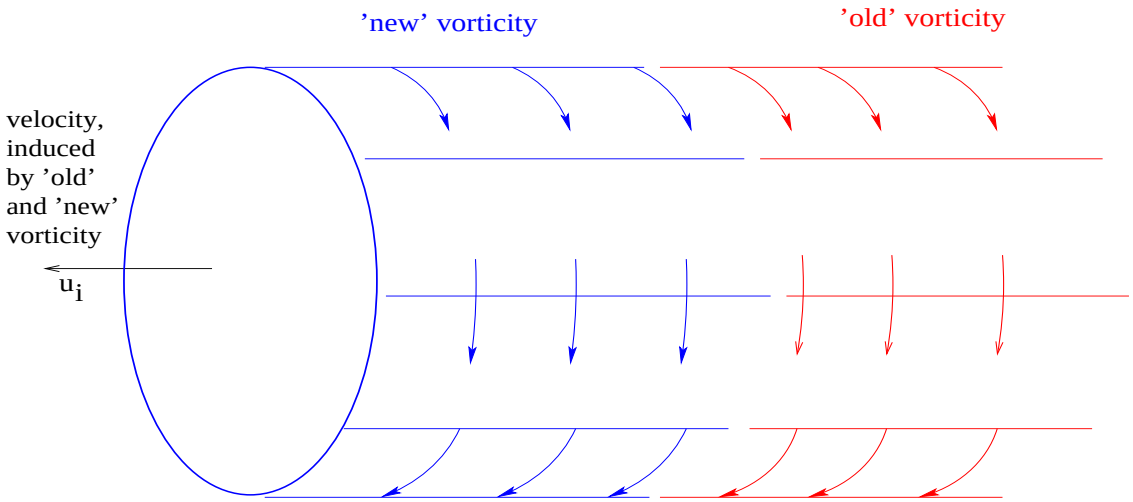


Figure 2: Wake with 'mixed' vorticity as a result of e.g. a pitch angle step

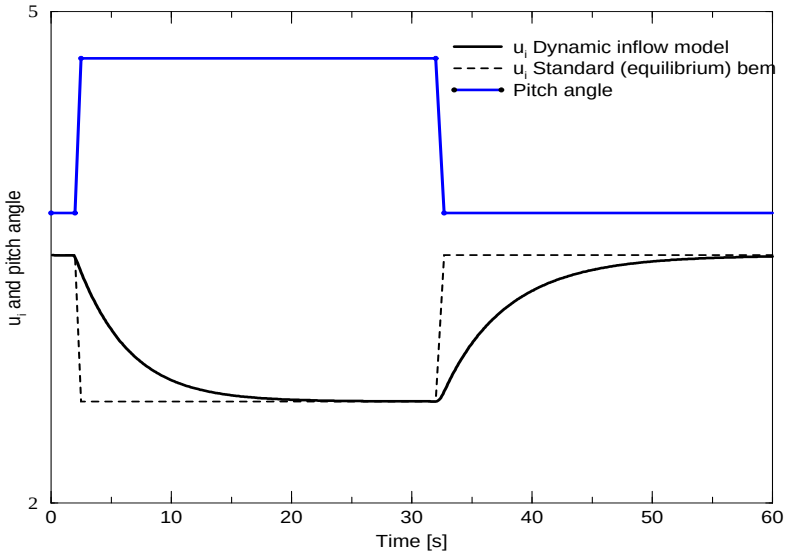


Figure 3: Induced velocity (qualitatively) in response to pitch angle step

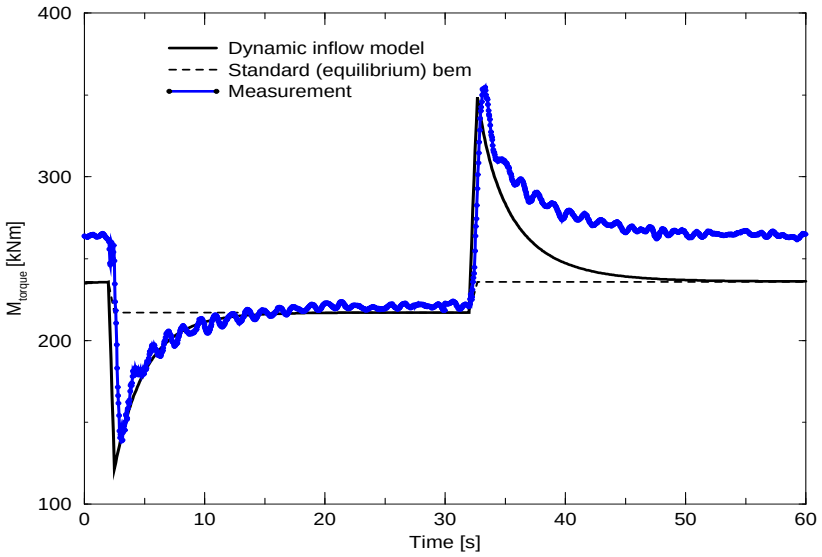


Figure 4: Rotor shaft torque on Tjæreborg turbine in response to pitch angle step

# 3 Description of NASA-Ames measurements at fast pitching steps

## 3.1 Instrumentation and conditions

The present project makes use of the dynamic inflow measurements which have been performed by the National Renewable Energy Laboratory NREL in the USA. A picture of the wind turbine placed in the NASA-Ames wind tunnel test section is shown in Figure 5. The wind tunnel is located in the NASA-Ames Research Center. The tunnel is open loop with a closed test section of 24.4x36.6 m. The tunnel speed is variable between almost zero and 50 m/s, where the NREL measurements were performed at tunnel speeds ranging between 5 and 25 m/s. As noted in [10] the turbulence intensity at a tunnel speed of 5 m/s is in the order of 2.5 %, where it decreases towards 0.2% at a tunnel speed of 24 m/s.

The main characteristics of the turbine are as follows:

- The rotor diameter is 10 m. This implies that 9% of the test section area is covered by the rotor plane. This is well below the 10% which is commonly considered to be acceptable for closed wind tunnel test sections. In [9] it is noted that the maximum blockage can be in the order of 2% but for the majority of the cases, the blockage is less than 1%;
- The turbine is 2-bladed (with blade numbers given as number 1 and **3**, note that blade number 3 is the instrumented blade);
- The blades have a linear taper with a maximum chord of 0.737 m at 25% span and 0.356m at 100% span. As already pointed out in [2] this results in a relatively low aspect ratio and high solidity compared to modern (2 bladed) wind turbines;
- The blades have a non-linear twist of 22.5 degrees over the blade;
- The airfoil is the S809 airfoil, over the entire span;
- The turbine has an asynchronous generator with a rated rotor speed of 72 rpm. For a 10 m rotor and for the present tunnel speeds, this results in a relatively low tip speed ratio.

One of the blades (blade number 3) was heavily instrumented at 5 radial positions with 22 pressure taps each. The measurement sections (relative to the rotor centre) are located at 30%, 47%, 63%, 80% and 95% span, i.e. at r= 1.510 m, 2.343 m, 3.185 m 4.023 m and 4.780 m. The resulting pressure distributions are integrated to normal forces and tangential forces.

In addition the inflow velocities and inflow angles are measured from five hole probes. These probes were placed 4% outboard of the pressure taps, i.e. at r= 1.710 m, 2.5653m, 3.370 m and 4.225 m and 4% inboard of the outer station, i.e. at r=4.5773 m. Note that the inflow measurements were not used in the present study.

For the purpose of dynamic inflow analysis, time series have been measured at fast stepwise pitch changes, similar to the ones which were measured by DTU in the Dynamic Inflow projects, see section 2.

The pitching steps have been performed at different tunnel speeds. Now it should be realised that dynamic inflow effects are expected to be most pronounced at relatively high values of the axial induction factor. As explained in [6] the highest axial induction factor is found at the lowest available tunnel speed, which is 5 m/s. Hence, the measurement series at this wind speed has been requested at NREL and will be analysed in the remainder of this report.

Figure 6 shows the measured time series of the pitch angle. The measurement period is 600 seconds and within this period 200 pitch angle steps are performed. Thereto the pitch angle is repeatedly increased with a fast pitching speed from a pitching angle of approximately -5.90

degrees to 10.02 degrees, after which it remains constant for some 15 s. Thereafter it decreases again to a pitch angle of -5.90 degrees.

As mentioned above, the dynamic inflow effects are expected to depend heavily on the value of the axial induction factors. For this purpose the axial induction factors have been calculated with PHATAS, see section 4.2. The results are shown in table 1 as function of radius.

It can be noted that the rotor is heavily loaded at a pitch angle of -5.90 degrees but at a pitch angle of 10.02 degrees the rotor is only very lightly loaded. As such the pitch angle steps should be considered as rather artificial but they are very suitable for validation purposes.

## 3.2 Processing of measurements

It should be realised that even in the present wind tunnel environment some fluctuations appear in the measured response which are not caused by dynamic inflow. These undesired fluctuations mainly result from (turbine dependent) structural dynamics.

Apart from the interference with structural effects, there are fluctuations from the tower shadow and from slight, inevatible instationarities in the wind tunnel conditions (as mentioned above, the turbulence intensity increases with decreasing tunnel speed where the current measurement series is selected at the lowest possible tunnel speed of 5 m/s). In order to smoothen the load signals an averageing procedure has been applied similar to the one from the Dynamic Inflow project, see section 2. Thereto the different pitchings steps are synchronised and initialised to the start of the pitching step transient. The resulting, synchronised, time series are then averaged in order to filter out the fluctuations as good as possible.

The averaged upward pitching step is given in Figure 7 and the downward pitching step is given in Figure 8. Note that the pitching step starts at t = 0 s.

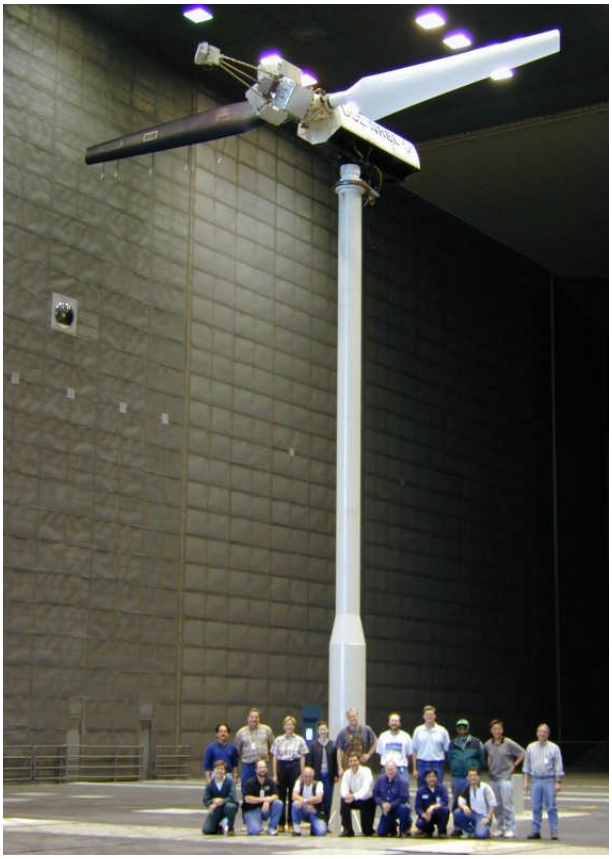

Figure 5: Wind turbine in wind tunnel

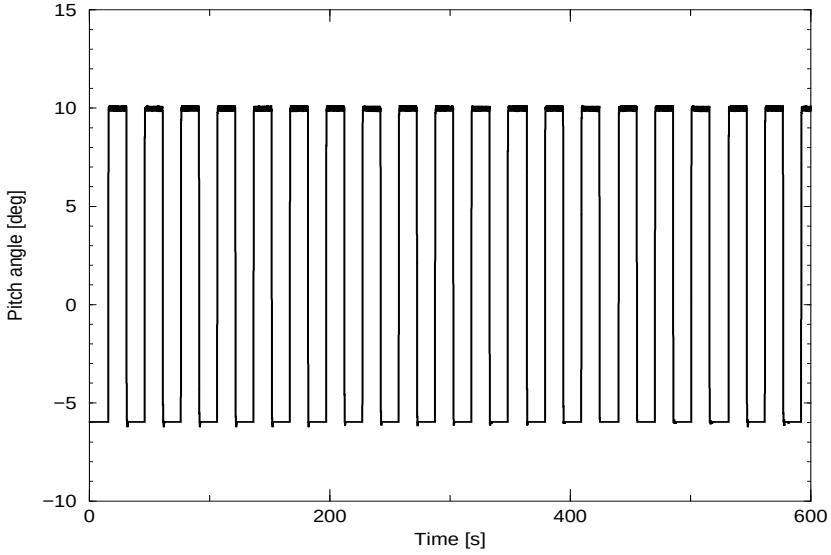


Figure 6: Pitch angle variation during 600 seconds

| pitch angle (deg) | $a_{30}$ [-] | $a_{47}$ [-] | $a_{63}$ [-] | $a_{80}$ [-] | $a_{95}$ [-] |
|---|---|---|---|---|---|
| -5.90 | 0.32 | 0.42 | 0.58 | 0.68 | 1.06232 |
| 10.02 | 0.039 | 0.005 | 0.008 | -0.0168 | -0.03 |

Table 1: Axial induction factor at a pitch angle of -5.9 degrees and 10.02 degrees

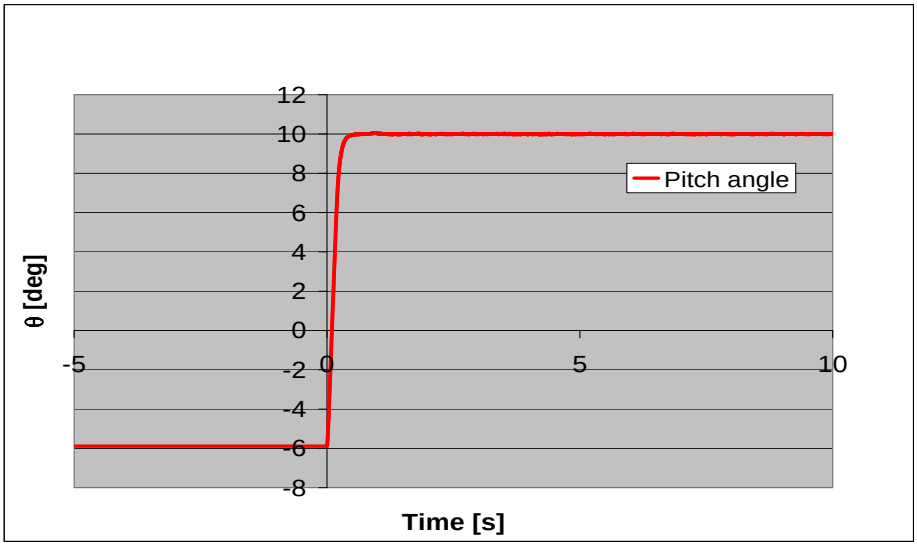


Figure 7: Upward pitching step, (Averaged over 10 realisations)

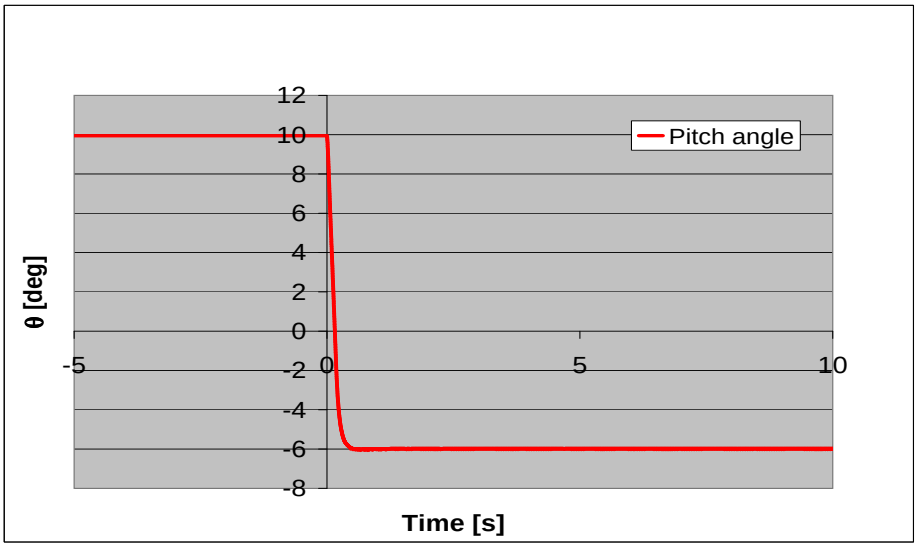


Figure 8: Downward pitching step, (Averaged over 10 realisations)

# 4 ECN models for dynamic inflow

In this section, the ECN models are described which have been used to simulate the dynamic inflow measurements from section 3. One of these models is of an 'engineering type', i.e. a model with a computational effort comparable to the conventional blade element momentum theory, where the other model is more elaborate and based on a free wake lifting line model. The engineering model is implemented in ECN's aero-elastic code PHATAS, [3].

## 4.1 Engineering model for dynamic inflow

A detailed description of the engineering model as implemented in PHATAS, is given in [5].

The model is derived from an integral relation which in turn is extracted from a simplified vortex wake sheet model. The simplified vortex wake model has the following features and assumptions:

- The blade is modelled as a vortex line from the rotor axis to the tip with a constant bound vortex strength $\Gamma$ along the radius. This approximation implies that:
  - All the vorticity which is trailed into the wake is concentrated at the tip and the root of the rotor but the root vorticity only induces velocities in tangential direction. These tangential velocities are of less relevance for the present study;
  - The bound vortex strength is related to the axial force coefficient $\mathrm{C_{D.ax}}$. Thereto it is assumed that the integral of the lift force over the blade length equals the axial force per blade, i.e.

$$\mathrm{F_{ax,blade}} \approx \int_0^{\mathrm{R}} \rho \mathrm{V_{eff}} \Gamma \mathrm{dr} \approx \rho \Gamma \int_0^{\mathrm{R}} \Omega \mathrm{r dr} = 0.5 \rho \Gamma \Omega \mathrm{R}^2 \tag{1}$$

$$\mathrm{F_{ax,blade}} = \mathrm{C_{D.ax}} 0.5 \rho \mathrm{V_w^2} \pi \mathrm{R}^2 / \mathrm{B} \tag{2}$$

  From equation 1 and 2, it follows that $\Gamma = \pi \mathrm{C_{D.ax}} \mathrm{V_w^2} / (\Omega \mathrm{B})$

- The bound vortex which is trailed from the tip of the blade is distributed over a semi-infinite cylinder sheet with radius R equal to the rotor radius. This implies that deformation (expansion) of the tip vortex is neglected. The trailed vorticity is decomposed into an axial and tangential component of the wake vorticity where it is the tangential component ($\gamma_\mathrm{t}$) which induces the axial velocities in the rotor plane. The tangential vorticity density is found by distributing the bound vortex strength over the distance which the vortex has transported until the next blade passes. The vorticity is transported with a velocity $\mathrm{V_{tr}}$ which remains constant throughout the wake and which is equal to the velocity with which it is trailed at the tip: $\mathrm{V_{tr}} = \mathrm{V_{wind}} - \mathrm{u_i}$.

- The axial velocities are calculated from the tangential vorticity density with the law of Biot-Savart. The resulting equation is an integral over the cylinder surface (with x the streamwise and $\phi$ the azimuthal coordinate):

$$\mathrm{u_i} = \frac{\mathrm{R}}{4\pi} \int_{\mathrm{x}=0}^{\infty} \int_{\phi=0}^{2\pi} \frac{\gamma_\mathrm{t}(\mathrm{x})[\mathrm{R} - \mathrm{r}\cos\phi]}{[\mathrm{x}^2 + \mathrm{R}^2 + \mathrm{r}^2 - 2\mathrm{rR}\cos\phi]^{3/2}} \mathrm{d}\phi \mathrm{dx} \tag{3}$$

- For equilibrium conditions (i.e. constant wind speed and $\mathrm{C_{D.ax}}$) the bound vortex strength and the resulting wake vorticity are constant. Hence $\gamma_t$ can be placed outside the integral in

equation 3. This makes it possible to solve equation 3 analytically. The final solution turns out to be the well known momentum theory equation:

$$C_{D.ax} = 4a(1-a) \tag{4}$$

where the axial induction factor a is constant along the rotor plane.

For non-equilibrium situations, the term $\gamma_t(x)$ should be placed inside the integral of equation 3. For this situation, no analytic solution is known. However, by differentiation of equation 3 and reasoning that the correct steady state solution should be obtained, the following equation is constructed for the axial induced velocity at radius r:

$$4Rf_a\frac{d}{dt}(u_i) + 4u_i(V_w - u_i) = \sigma V_{eff}^2 c_n$$

In all cases which are analysed in the present study, the tunnel speed is constant. For these conditions the expression can be written as a first order differential equation in time on the axial induction factor:

$$\frac{R}{V_w}f_a\frac{da}{dt} + a(1-a) = C_{D.ax}/4 \tag{5}$$

Note that $C_{D.ax}$ is the axial force coefficient on a rotor annulus at radius r.

The time constant $\tau = \frac{R}{V_w}f_a$ contains the term $f_a$ which is a function of the radial position and found to be:

$$f_a = 2\pi / \int_0^{2\pi} \frac{[1-(r/R)\cos\phi]}{[1+(r/R)^2 - 2(r/R)\cos\phi]^{3/2}} d\phi \tag{6}$$

It can be noted that:

- Equation 5 contains the non-linear term $a^2$. This term is often relatively small ($a \approx 0.33$)
- For equilibrium conditions, the time derivative in equation 5 is zero and as expected, the instationary equation returns to the stationary momentum equation 4;
- In figure 9 the term $f_a$ is plotted as function of r/R. It can be seen that its value is 1 in the rotor centre leading to a time constant of $\tau = R/V_w$. The time constant gets shorter towards the tip. This is due to the fact that the outer portions of the blade are close to the tip vorticity. The outboard positions of the blade are then, through the law of Biot and Savart, more sensitive to a change in tip vorticity.

## 4.2 PHATAS

The engineering model, as described in section 4.1, has been implemented in ECN's code PHATAS. The calculations in the present report have been performed with PHATAS release "Apr-2005b". This version of the code is described in [3]. The aerodynamic modelling of this version is reported in chapter 5 of [2].

The following remarks can be made on the PHATAS simulations:

- The input on the NREL wind turbine is based on the description given in [2]. Several degrees of freedom are taken into account, e.g. the blade flexibility in the edgewise and flatwise direction, blade torsion, shaft torsion and the dynamics of the tower. Furthermore the asynchronous generator has been modelled;

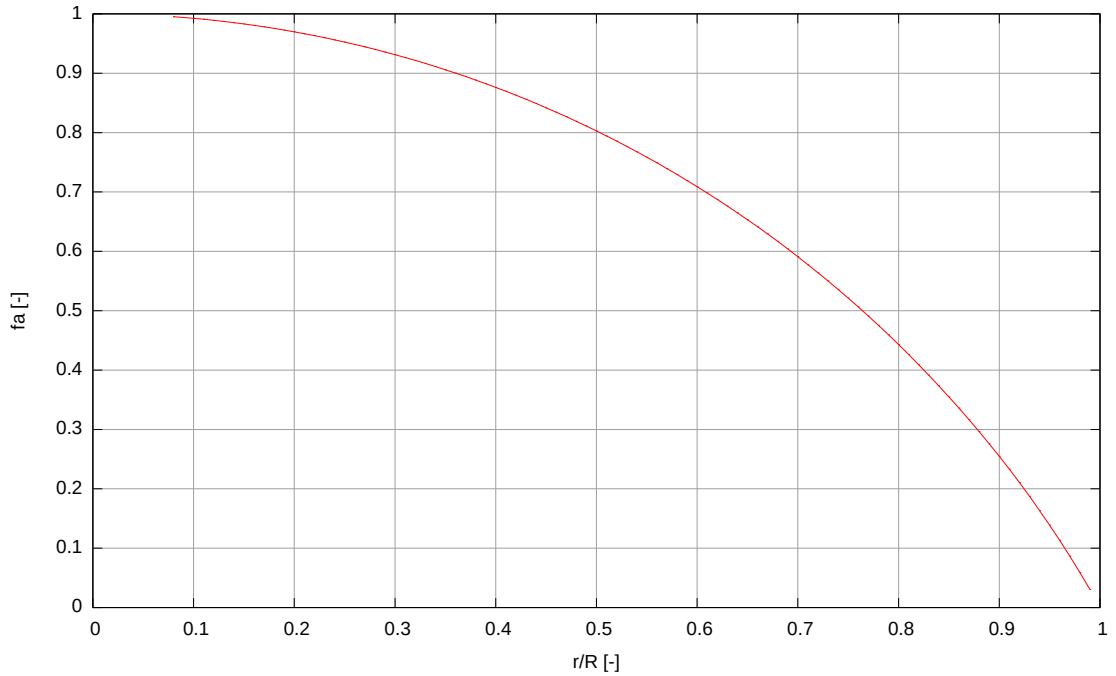


Figure 9: Factor $f_a$ as function of radial position

- The tunnel speed is assumed to be homogenous and constant in time, but tower shadow has been included;
- The aerodynamic modelling of PHATAS is based on the blade element momentum theory. This requires tables of aerodynamic characteristics (i.e. $c_l(\alpha)$, $c_d(\alpha)$ and $c_m(\alpha)$ curves). It is noted that the aerodynamic airfoil of the wind turbine is the NREL S809 airfoil along the entire blade. The 2D, stationary (non-rotating) aerodynamic characteristics of this airfoil have been constructed by combining 2D wind tunnel measurements from the University of Delft with wind tunnel data from Ohio State University. The data have been extended to deep stall according to the methodology as described in chapter 2 of [2]. The resulting 2D aerodynamic characteristics are presented in Figures 10 and 11 .
- Dynamic stall effects (which may play a role at the downward pitching step, see section 6), are modelled with the first order dynamic stall model from [4].

## 4.3 Free wake model, AWSM

The AWSM code, see [1], is based on a non-linear lifting line vortex wake theory. The code is of a free wake character by which it is capable of modelling the vorticity representation of dynamic inflow from section 2 in a more physical correct way. It is noted that for distances larger than 4 rotor diameters downstream of the rotor, the wake is treated as 'frozen'.

The blades are modelled as lifting lines. This implies that, similar to the PHATAS code, aerodynamic profile data should be prescribed as function of the angle of attack. Thereto the same airfoil data as used in PHATAS have been applied. 3D and dynamic stall corrections are not taken into account (although instationary effects which result from the shed vorticity are modelled).

The AWSM calculations were made under the following assumptions:

- The construction is assumed to be rigid and mass induced loads are neglected;

- The wind speed is constant in time and homogenous;
- The aerodynamic tower shadow effect has been neglected;
- The rotor speed is constant.

Finally it is noted that several improvements were made to the AWSM code, mainly on the numerics, in order to make the code robust for the present, rather artificial, pitching steps.

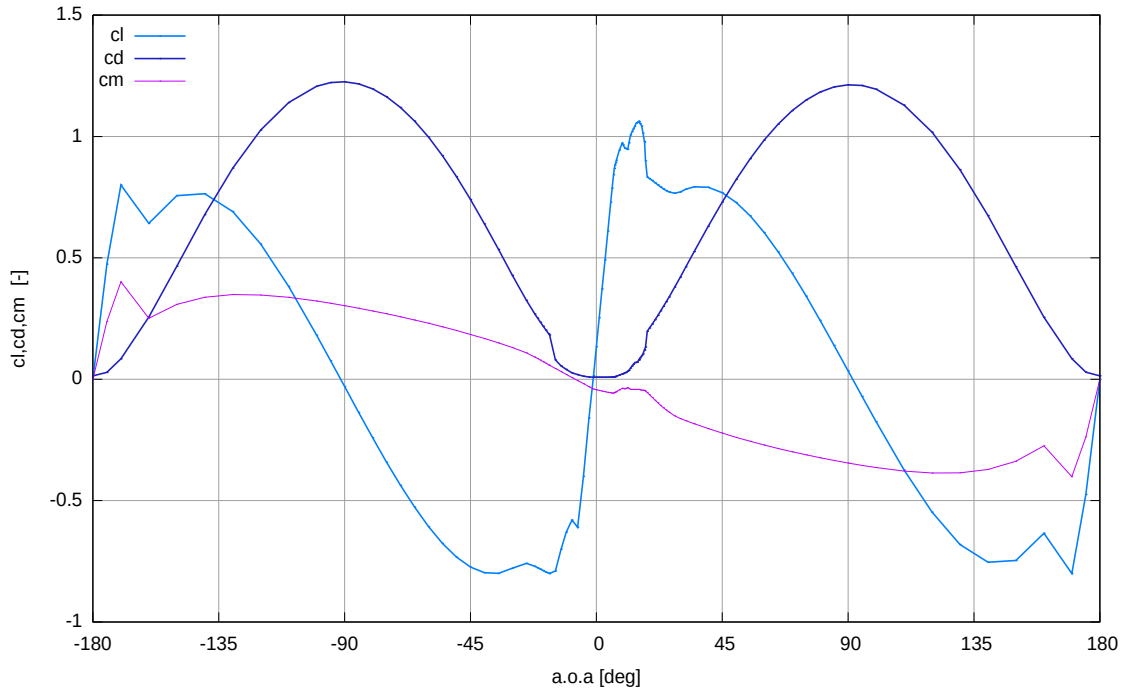


Figure 10: S809 airfoil: Basic 2D aerodynamic coefficients for -180 < $\alpha$ < 180

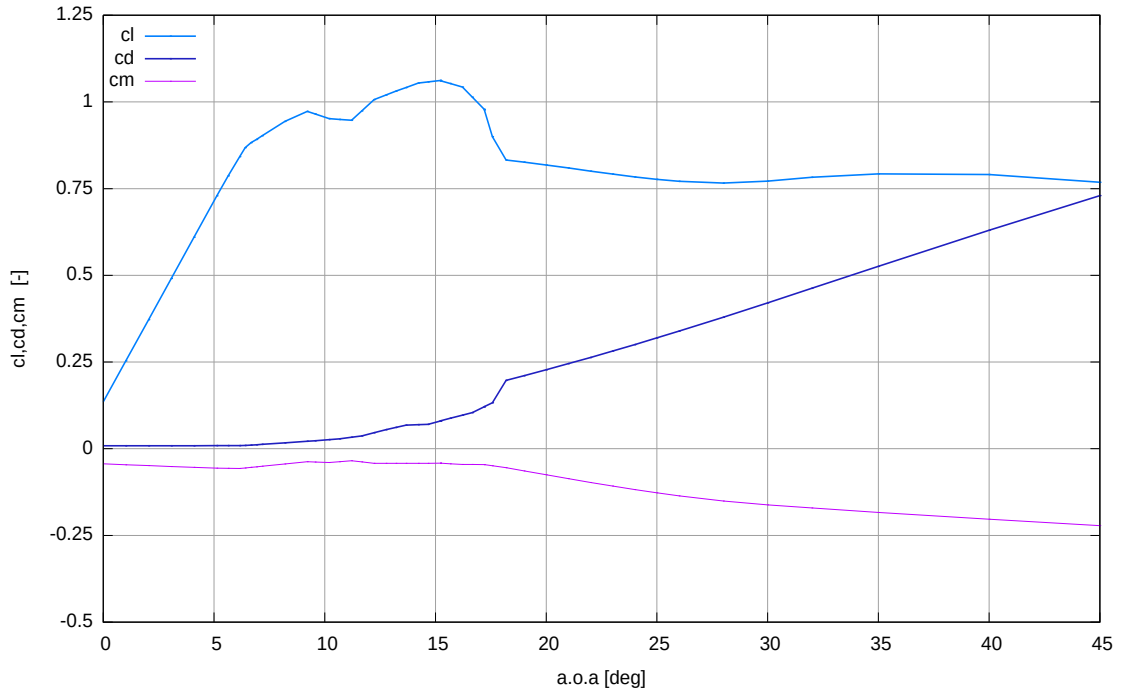


Figure 11: S809 airfoil: Basic 2D aerodynamic coefficients for 0 < $\alpha$ < 45

# 5 Comparison between calculations and measurements

In this section the measurements (averaged in the way as described in section 3.2) are compared with calculational results from the aero-elastic code PHATAS (which includes the engineering model from section 4.1) and the free wake lifting line method AWSM.

The pitch angle transients as prescribed to the codes are based on the measured pitch angle transients (Figures 7 and 8). Thereto the measured transient is approximated by an instantaneous pitch angle step with a constant pitching speed of 56.8 degrees/seconds. This implies that the pitching step is completed within 0.28 seconds. The actual pitching step lasts slightly longer because it is 'shaved' at the start and the end of the pitching step.

Figures 12 to 15 show the comparion between calculated and measured blade and rotor loads (i.e. the flatwise moment and rotorshaft). In this comparison the results from the AWSM-code are not presented. In section 6 it will be shown that these loads are strongly influenced by structural dynamic effects, but these effects are not included in the AWSM code.

Figures 16 to 25 show the comparison in terms of local normal forces, perpendicular to the chord.

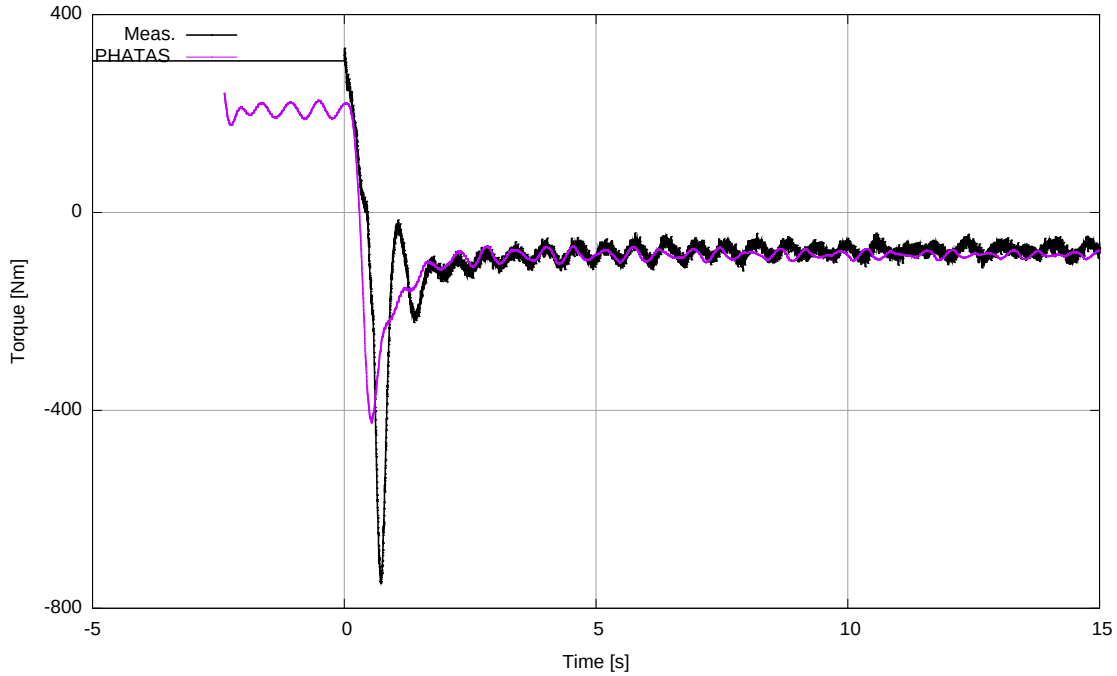


Figure 12: Torque: Comparison between measured and PHATAS calculated results: Upward pitching step

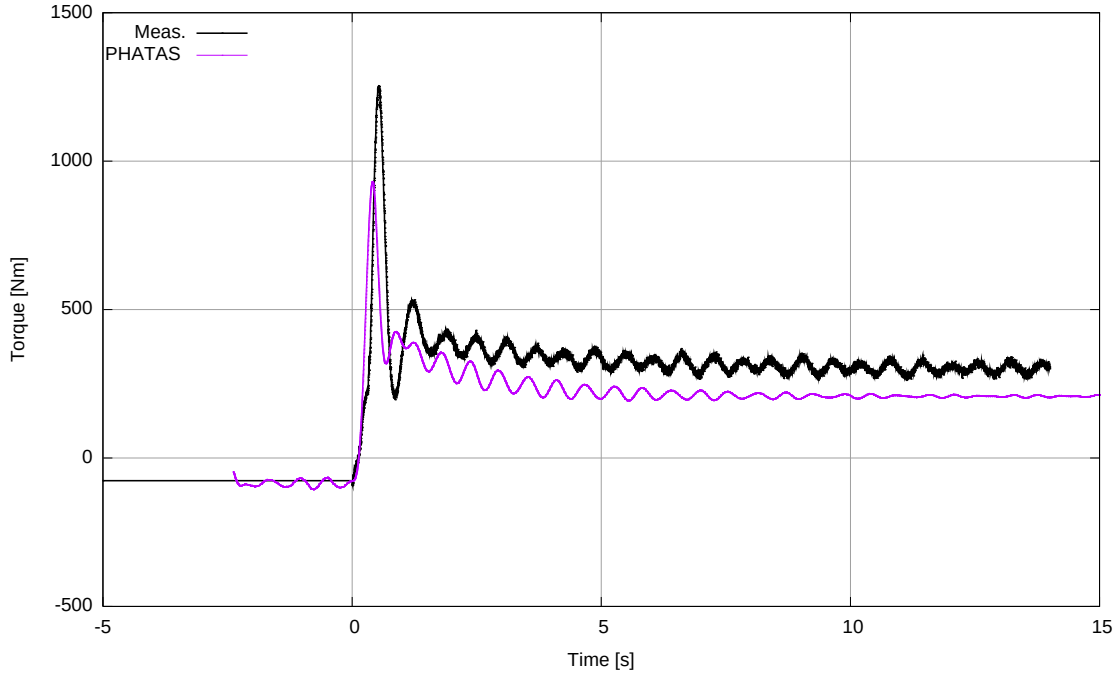


Figure 13: Torque: Comparison between measured and PHATAS calculated results: Downward pitching step

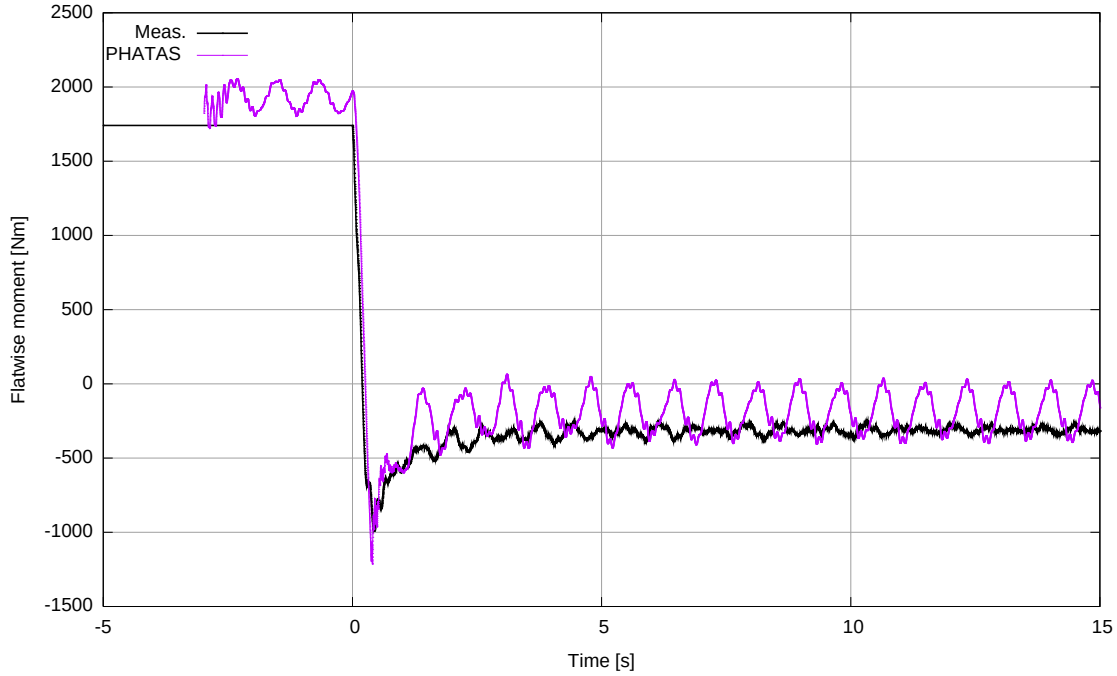


Figure 14: Flatwise moment: Comparison between measured and PHATAS calculated results: Upward pitching step

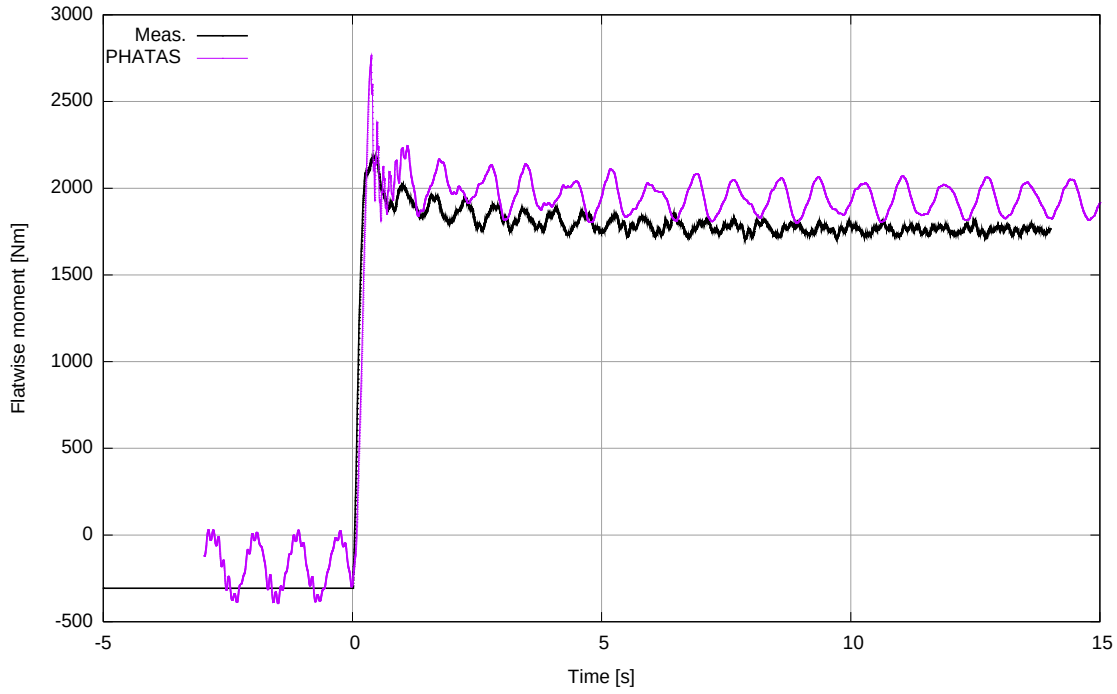


Figure 15: Flatwise moment: Comparison between measured and PHATAS calculated results: Downward pitching step

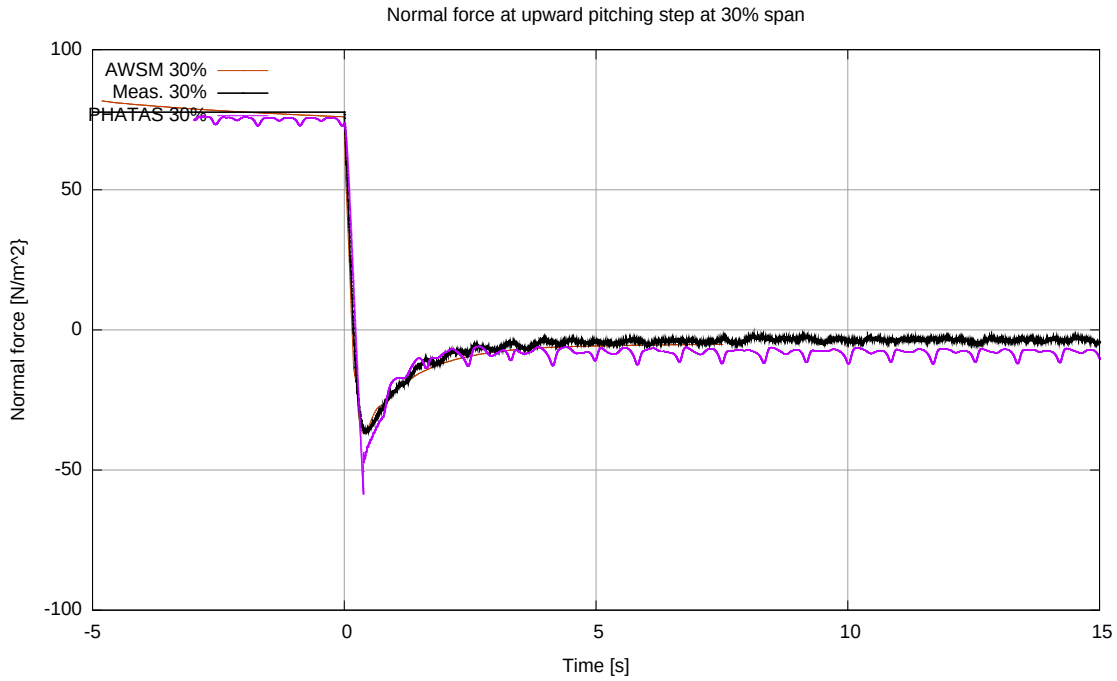


Figure 16: Upward pitching step: normal force at 30% span: Comparison between measured and calculated results

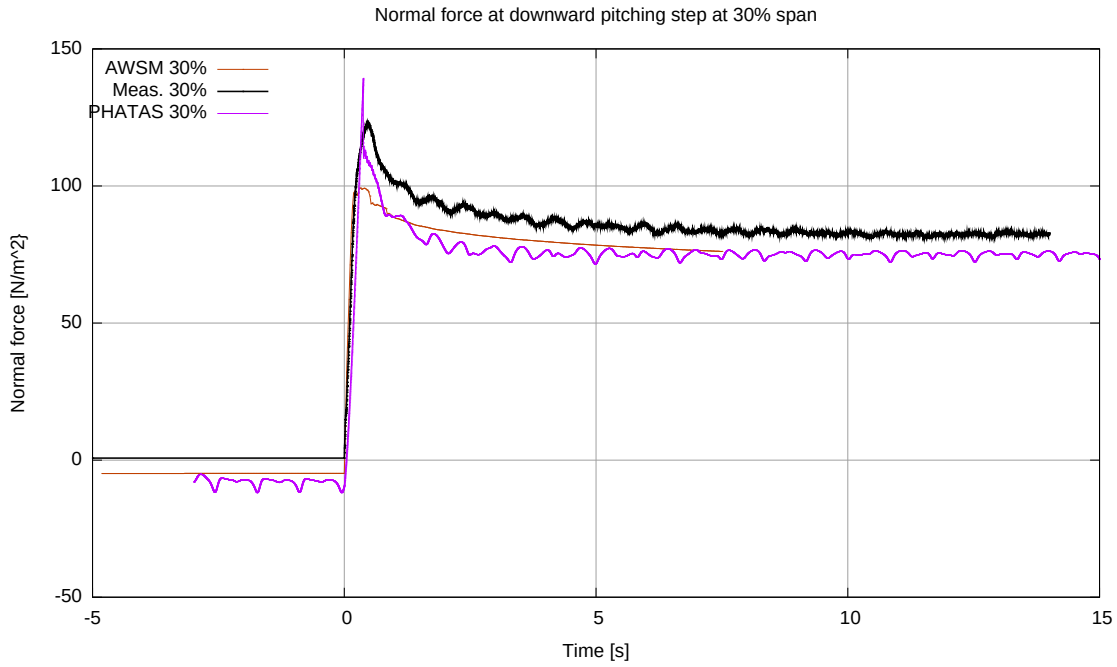


Figure 17: Downward pitching step: normal force at 30% span: Comparison between measured and calculated results

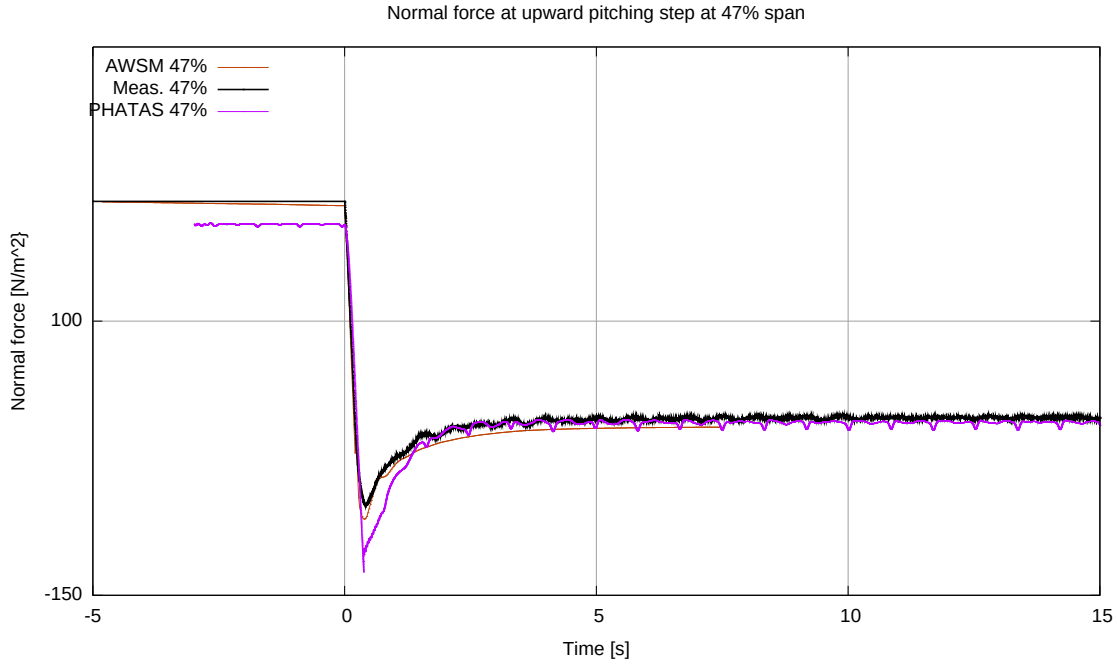


Figure 18: Upward pitching step: normal force at 47% span: Comparison between measured and calculated results

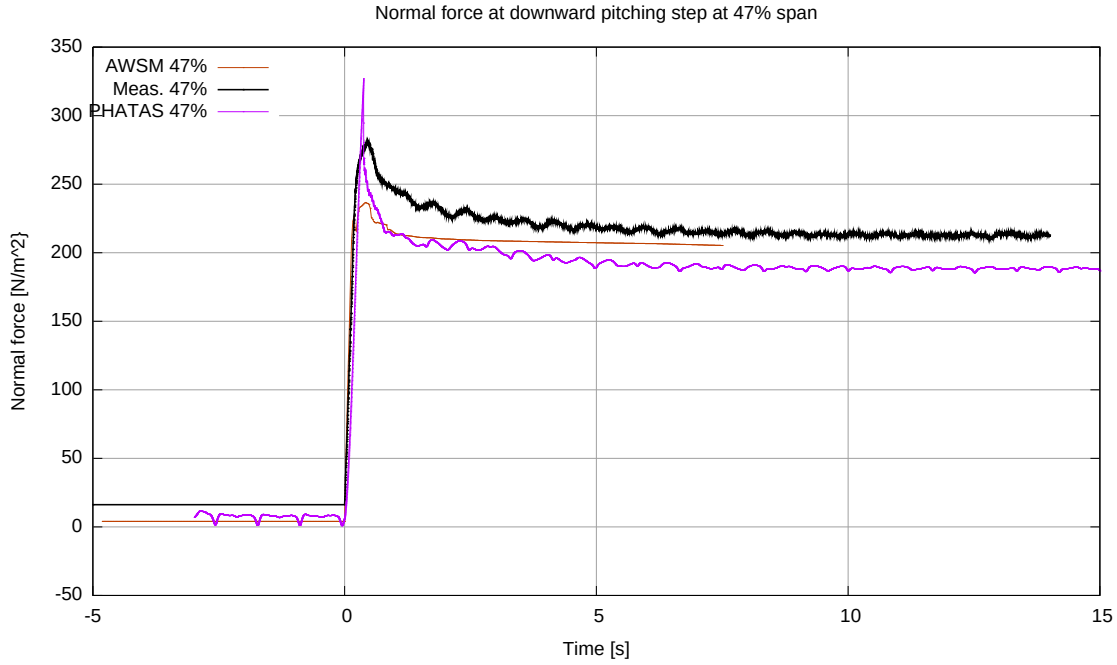


Figure 19: Downward pitching step: normal force at 47% span: Comparison between measured and calculated results

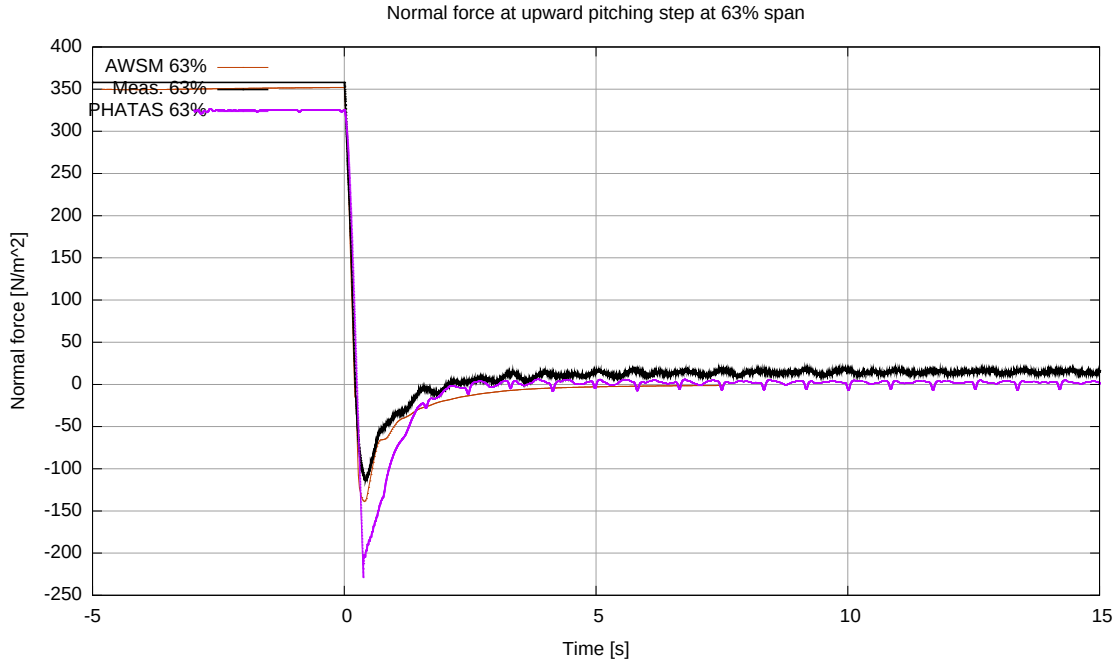


Figure 20: Upward pitching step: normal force at 63% span: Comparison between measured and calculated results

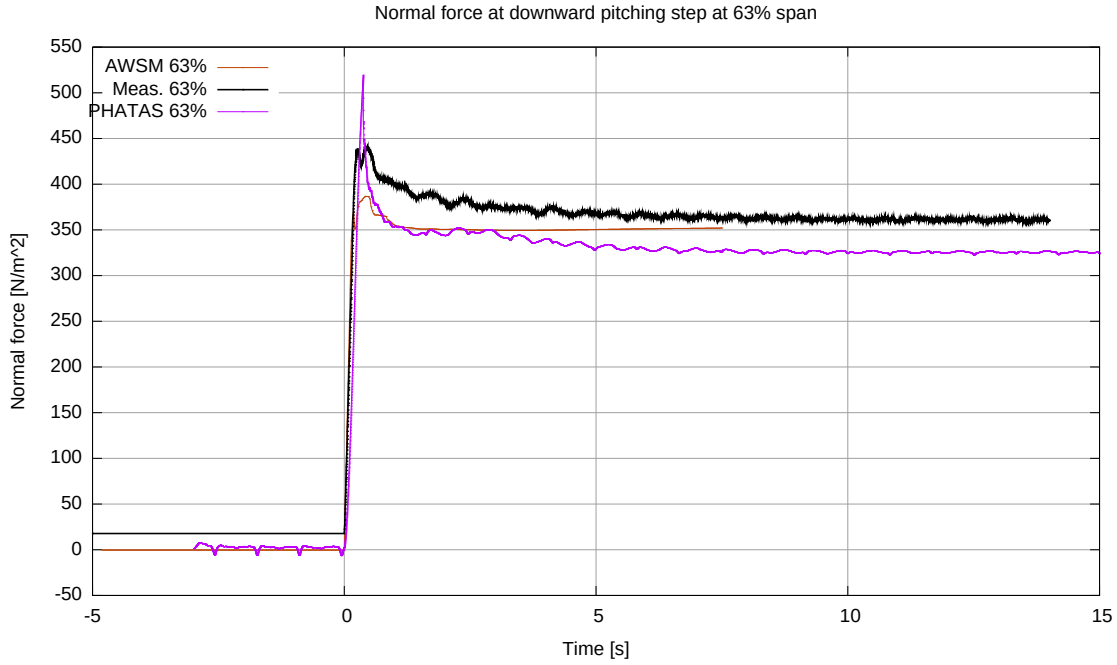


Figure 21: Downward pitching step: normal force at 63% span: Comparison between measured and calculated results

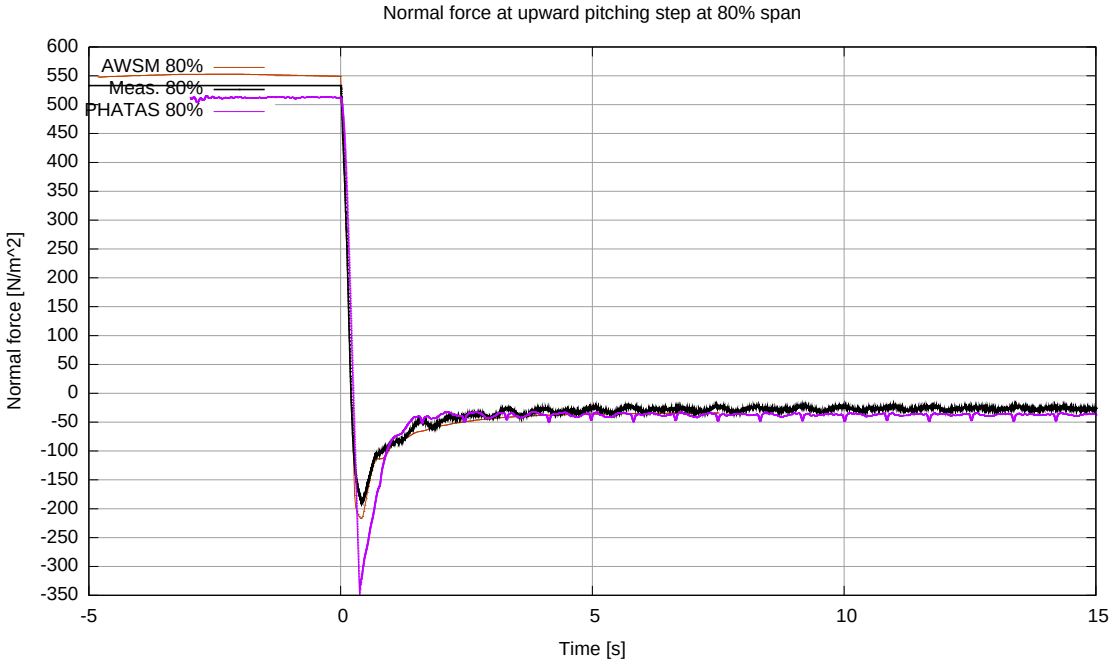


Figure 22: Upward pitching step: normal force at 80% span: Comparison between measured and calculated results

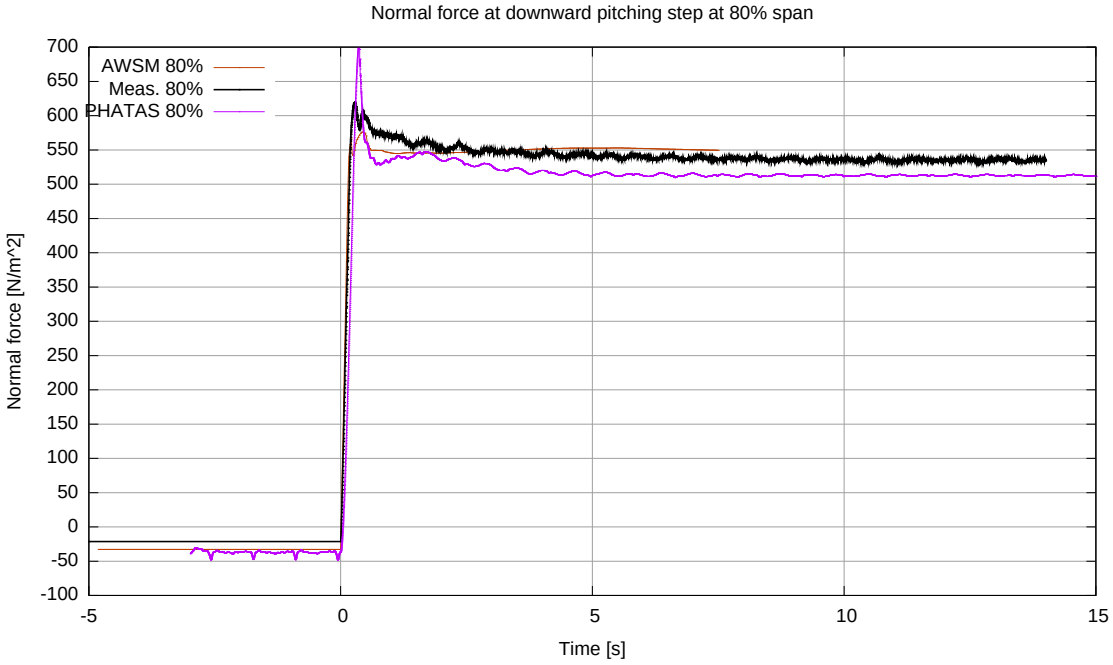


Figure 23: Downward pitching step: normal force at 80% span: Comparison between measured and calculated results

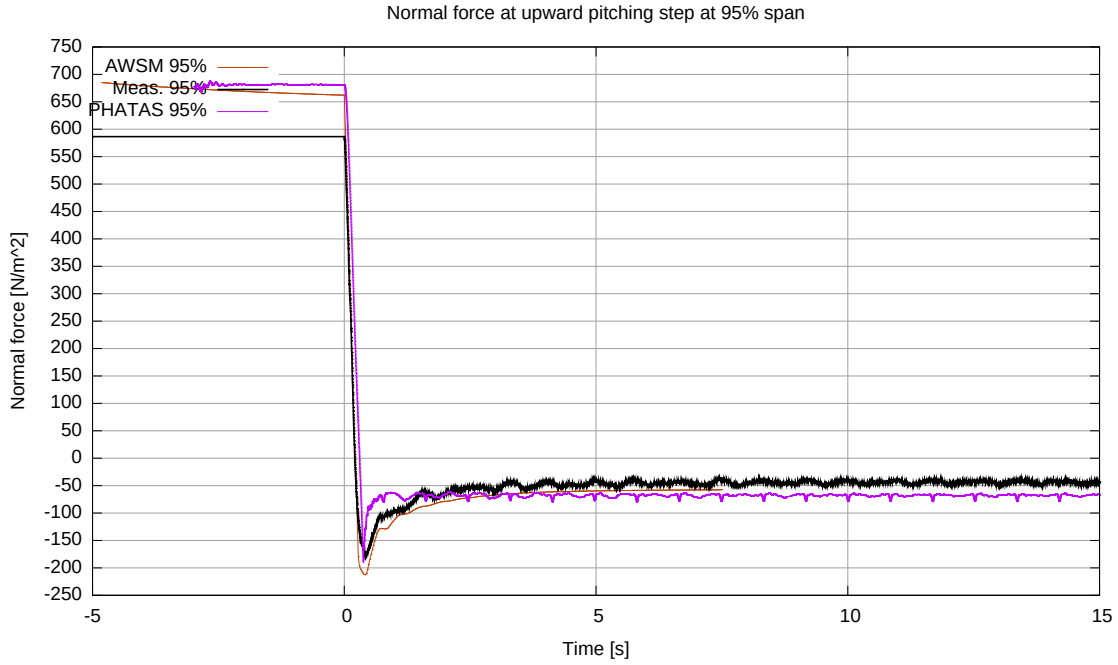


Figure 24: Upward pitching step: normal force at 95% span: Comparison between measured and calculated results

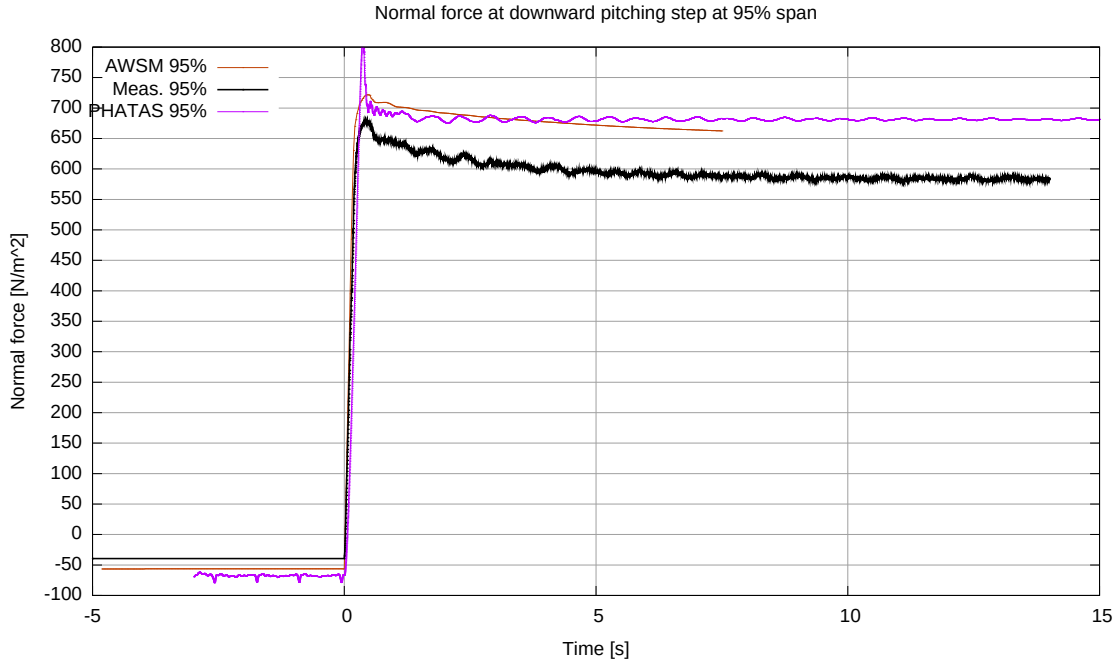


Figure 25: Downward pitching step: normal force at 95% span: Comparison between measured and calculated results

The following observations can be made :

- In all (measured and calculated) transients, the effects from dynamic inflow are clearly visible. Just after the pitching step a load overshoot appears, after which it takes a certain period in time before the new equilibrium value is reached. This resembles very much the behaviour of the loads which were measured in the European Dynamic Inflow projects, see section 2. The dynamic inflow effects donot only appear in the rotor(blade) loads of Figures 12 to 15 but also in the sectional normal forces. The 'high frequency' fluctuations which appear in the rotorshaft torque are a result of the rotorshaft flexibility, see section 6. Qualitatively speaking they are reproduced well by PHATAS, although the overshoot is underpredicted.

- At first sight it might be expected that the dynamic inflow effects for the downward pitching step are the 'reverse' of the dynamic inflow effects for the upward pitching step. However, the dynamic inflow effects for the downward pitching step seem to be less pronounced (in terms of load overshoots). This may be a result of the overhoot in angle of attack just after the downward pitching step which gives values above the stall angle of attack ($\alpha_{\mathrm{stall}} \approx 9.5$ degrees (Figure 26). At these angles of attack the $\mathrm{c_l} - \alpha$ curve is relatively flat by which the overshoots are damped. At the upward pitching step (Figure 27), the angle of attack remains within the linear $\mathrm{c_l} - \alpha$ range.

  Another difference between the upward and downward pitching step is given by the fact that prior to the upward pitching step the axial induction factor is high, see table 1. This implies significant wake expansion and a relatively low downward convection velocity of the vorticity in the wake. This is followed by an increase in pitch angle which yields a gradual decrease of induced velocity. At the end of the transient the axial induction factor is very low which implies little wake expansion and a rapid convection of the 'new' vortices. As such the upward pitching step starts with a 'slow' dynamic inflow process. For a downward pitching step the situation is opposite. It starts with a 'rapid' dynamic inflow process with little wake expansion but at the end of the transient the convection velocity is low and the wake is more strongly expanded.

- Modelling of stalled conditions is known to be much more difficult than modelling of attached flow conditions. At stalled conditions strong 3-dimensional and instationary effects. In principle these effects are included in PHATAS but it is well known that these models suffer from uncertainties (see [6] and [7]. AWSM has not included a model for stall effects (and structural dynamic effects) at all. This then explains the larger differences between calculated and measured overshoots for the downward pitching step, where the stalling angle of attack is exceeded.

- For the upward pitching step, the agreement between measured and AWSM calculated results is excellent. It is not only the equilibrium levels which are predicted very well (this was already expected from the comparison between AWSM results and measurements at 'standard' conditions, see [6]) but the load overshoot and the time constant are also predicted well (note that the time constant is still assessed from visual inspection. A quantitative assessment of the time constant is carried out in chapter 7).

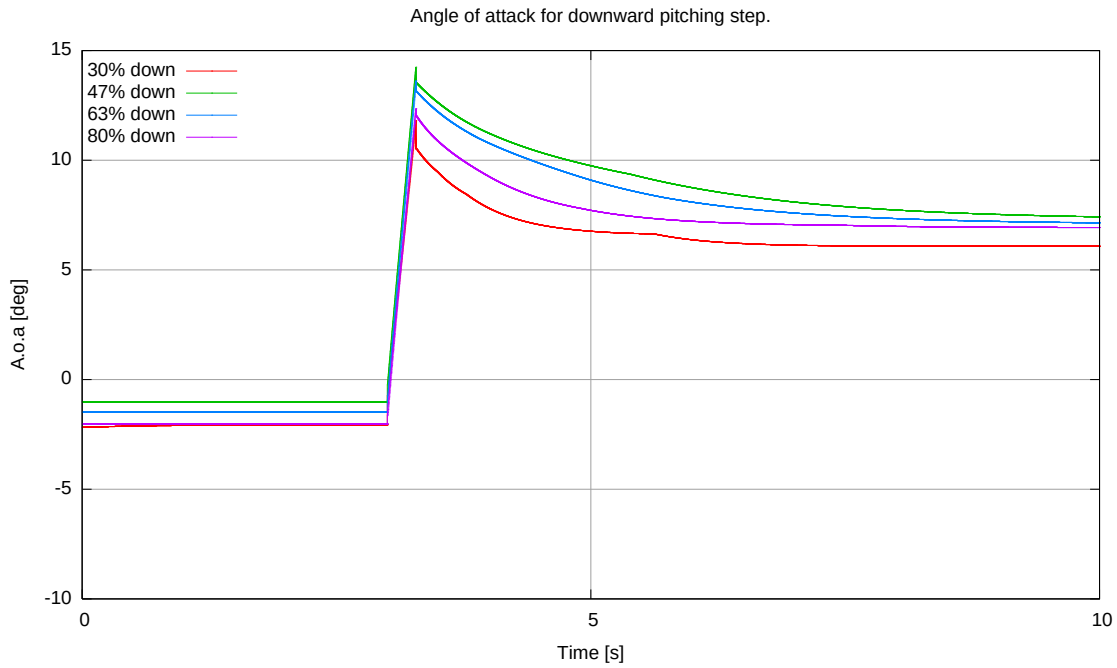


Figure 26: Downward pitching step: Angle of attack calculated by PHATAS

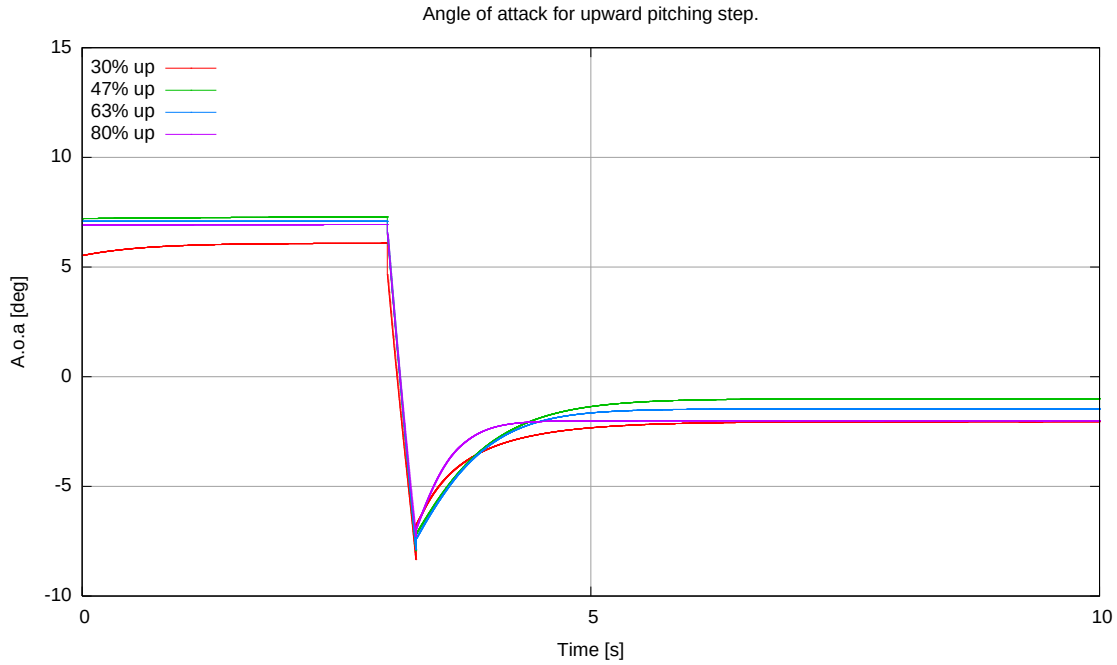


Figure 27: Upward pitching step: Angle of attack calculated by PHATAS

# 6 Effect of dynamic stall and structural flexibility

The present study focusses on an investigation of dynamic inflow. Nevertheless some of the fluctuations which appear in the figures from section 5 may have a different cause. One can think of structural dynamic effects or dynamic stall effects. The fluctuations from these effects may then interfere with the dynamic inflow fluctuations. A sensitivity study, performed with PHATAS showed that the effect from dynamic stall is very small on all predictions for either the upward or the downward step. Furthermore, the effects of blade flexibilities in flapping, edgewise and torsional direction, are negligible for most loads. This is not true however for the effect of shaft torsion flexibility on the rotorshaft torque, see Figure 28. This degree of freedom leads to strong fluctuations just after the step on the pitch angle. Similar fluctuations are found in the measured results, see Figures 13 and 12.

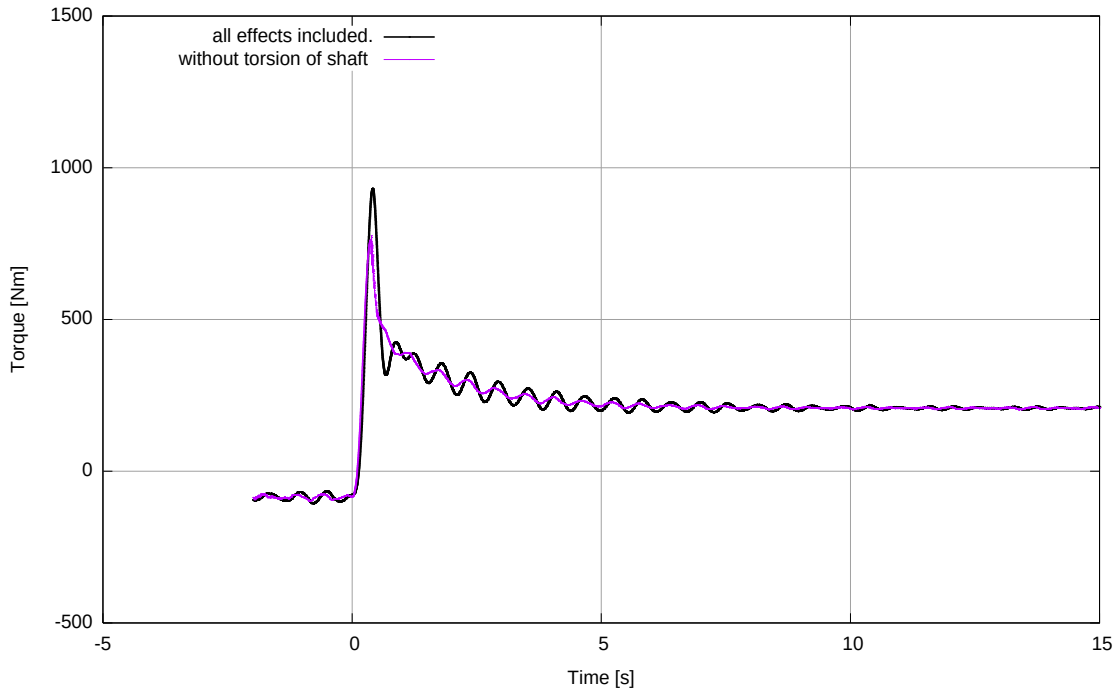


Figure 28: PHATAS calculated rotorshaft torque for downward pitching step: With and without torsional flexibility of the rotorshaft

# 7 Time scale analysis

The time constant is a very important parameter in the dynamic inflow process. A short time constant implies that the new equilibrium value is reached shortly after the change in rotor state and as such the event can still, with a reasonable agree of accuracy, be predicted with an equilibrium wake model. A longer time constant implies a longer response time by which the actual response will deviate from the response calculated with an equilibrium wake model.

Therefore a reliable assessment of the time constant is of utmost importance but the quantification of a time constant from the measured signals is not straightforward. Among other things, the definition of the time constant needs to be clarified. As a starting point, the induced velocity (i.e. the axial induction factor) is assumed to behave according to equation 5. By neglecting the quadratic $\mathrm{a}^2$ term, this equation becomes:

$$\tau \mathrm{da/dt} + \mathrm{a} = \frac{1}{4} \cdot \mathrm{C_{D.ax,2}} \tag{7}$$

with $\tau$ the time constant and $\mathrm{C_{D.ax,2}}$ the axial force coefficient on the annulus after the step in pitch angle. In addition it is assumed that $\mathrm{C_{D.ax,2}}$ is reached instantaneously after the step on the pitch angle (i.e. $\mathrm{C_{D.ax,2}}$ is independent of time).

Then equation 7 yields:

$$\frac{\mathrm{da}}{0.25\mathrm{C_{D.ax,2}} - \mathrm{a}} = \mathrm{dt}/\tau \tag{8}$$

With $0.25\mathrm{C_{D.ax.2}} = \mathrm{a_2}$ and $\Delta\mathrm{a} = \mathrm{a_2} - \mathrm{a_1}$, see Figure 29 in which $\mathrm{a_1} = \mathrm{a(t_1)}$ i.e. the initial value of a at t = $\mathrm{t_1}$, the following expression is found for the axial induction factor as function of time:

$$\mathrm{a(t)} = \mathrm{a_2} - \Delta\mathrm{a} \cdot \exp^{-(\mathrm{t}-\mathrm{t_1})/\tau} \tag{9}$$

Finally it is assumed that the variations in the blade loads are fully driven by the change in the axial induction factor. Then the transient of the load F(t) can be expressed in a form similar to equation 9:

$$\mathrm{F(t)} = \mathrm{F_2} - \Delta\mathrm{F} \cdot \exp^{-(\mathrm{t}-\mathrm{t_1})/\tau} \tag{10}$$

In this equation $\mathrm{F_2}$ is the new equilibrium value of the load and $\Delta\mathrm{F}$ the load overshoot, i.e. the difference between $\mathrm{F_2}$ and $\mathrm{F_1}$, with $\mathrm{F_1}$ the load just after the pitching step. Then equation 9 gives the following expression for the time constant:

$$\tau = -\frac{\mathrm{t} - \mathrm{t_1}}{\ln((\mathrm{F_2} - \mathrm{F(t)})/\Delta\mathrm{F})} \tag{11}$$

Hence equation 11 shows that the time constant can be determined from the actual value of the load F(t), the final equilibrium value $\mathrm{F_2}$ and the 'starting value' $\mathrm{F_1}$ (at $\mathrm{t_1}$). All of these values can in principle be extracted from the measured data. It should be realised however, that the determination of the time constant requires a very smooth and well defined dynamic inflow transient where even the present signals, though filtered and measured in the relatively stable wind tunnel environment, do show some fluctuations. This is in particular true for the rotorshaft torque (and to a smaller degree) the flatwise moment, see section 6. For this reason it is only the time constant of the normal forces which are determined in the present study. Furthermore equation 11 assumes $\tau$ to be a time constant. However, in the European Dynamic Inflow projects it was found, that the above mentioned assumptions are too crude for $\tau$ being a constant. For this reason the factor $\tau$ should be replaced by a time scale f(t), which is a function of time.

In table 2 the time scale for the upward step is given. The measured results are compared with the

time scale which is derived from the AWSM results and with the time scale from the engineering model, see equation 6. The measured and AWSM time scales are averaged over the period from t= 0.7 s to 3.7 s. In this period the time scale is believed to be most accurate. Thereto it should be realised that the time scale needs to be determined in a period which is not too short and not too long after t=$t_1$: In the period very shortly after t=$t_1$, equation 11 gives non-sensical results (i.e. $\approx$ 0/0). On the other hand, for t » $t_1$, the value of F(t) approaches $F_2$ and the argument in the log function approaches zero.

A graphical presentation of the measured time scale in the period from t= 0.7 s to 3.3 s is given in Figure 30 for the normal force at 30% span. Within this period the time scale turns out to be reasonable (though not completely) constant. A check on the validity of the resulting time scale is given in Figure 31. In this figure, the measured transient is compared with the transient from equation 10 using the time scale from table 2. The figure shows a very good fit.

Table 2 show a good agreement between the measured time scale and the time scale from the engineering model at the 30% and 47% section. This also appears from visual inspection in Figures 16, 18.

However the most important conclusion from table 2 is that the rapid decrease of the time scale towards the tip from the engineering model appears to a much smaller extent in the measured time scale. The decrease in time scale towards the tip from the AWSM calculated transients is qualitatively in very good agreement with the measurement although the time scale is consistantly longer (in the order of 0.25 s) at all radial positions.

As expected, the calculated and measured time scale results for the downward pitching step, show a poor agreement, see table 3.

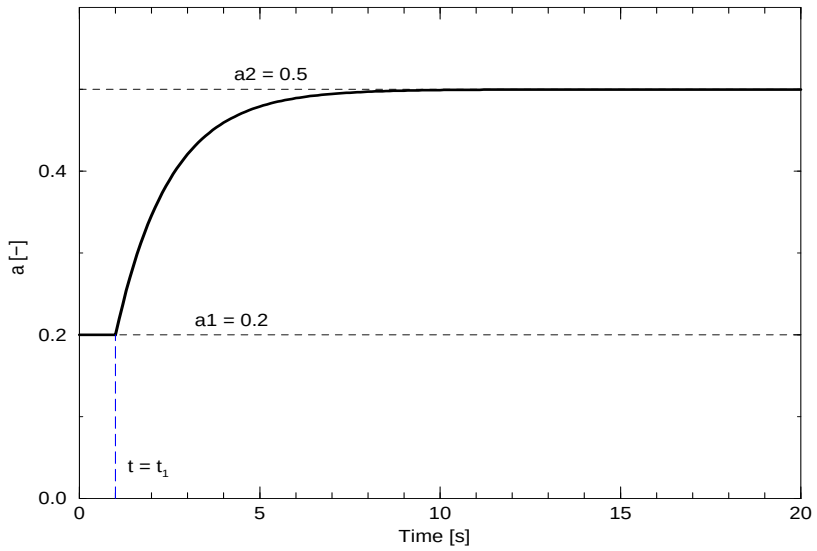


Figure 29: Assumed exponential behaviour of the axial induction factor

| r/R | $f_{up,meas}$ | $f_{AWSM}$ | $f_{analytic}$ |
|---|---|---|---|
| [-] | [s] | [s] | [s] |
| 0.30 | 0.95 | 1.12 | 0.93 |
| 0.47 | 0.83 | 1.04 | 0.83 |
| 0.63 | 0.77 | 1.01 | 0.68 |
| 0.80 | 0.74 | 1.00 | 0.44 |
| 0.95 | 0.78 | 1.03 | 0.14 |

Table 2: Upward pitching step: Time scale from measurements, AWSM calculations and from engineering model (averaged from t=0.7 s to t=3.7 s)

| r/R | $f_{down,meas}$ | $f_{AWSM}$ | $f_{analytic}$ |
|---|---|---|---|
| [-] | [s] | [s] | [s] |
| 0.30 | 1.07 | 1.98 | 0.93 |
| 0.47 | 1.09 | 1.61 | 0.83 |
| 0.63 | 1.10 | n.r. *) | 0.68 |
| 0.80 | 1.13 | 1.14 | 0.44 |
| 0.95 | 1.53 | 2.36 | 0.14 |

* too strong deviation from exponential behaviour

Table 3: Downward pitching step: Time scale from measurements, AWSM calculations and from engineering model (averaged from t=0.7 s to t=3.7 s)

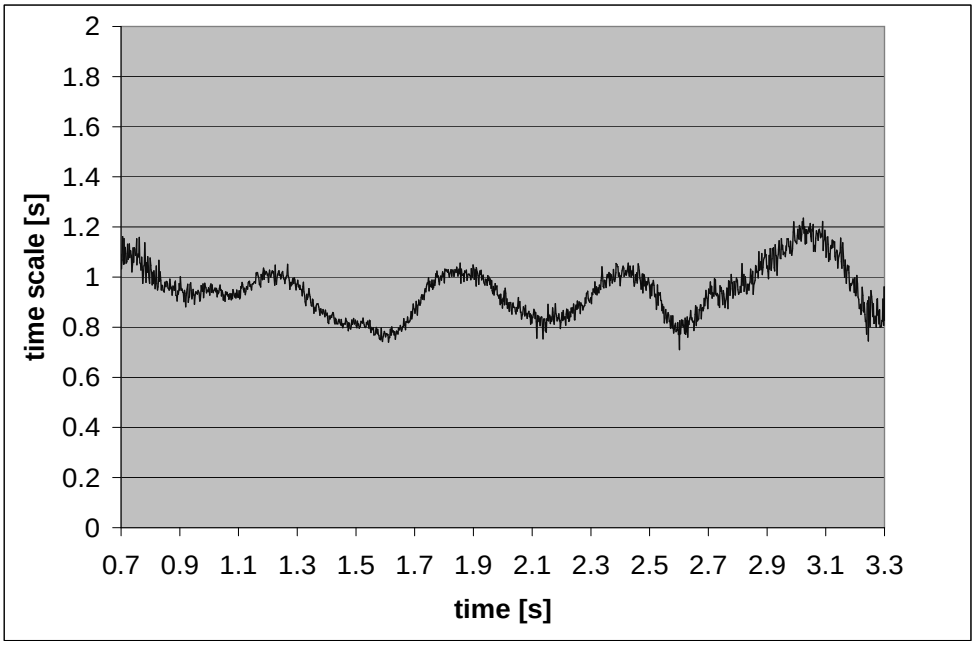


Figure 30: Time scale of normal force at 30% span as function of time (upward pitching stap)

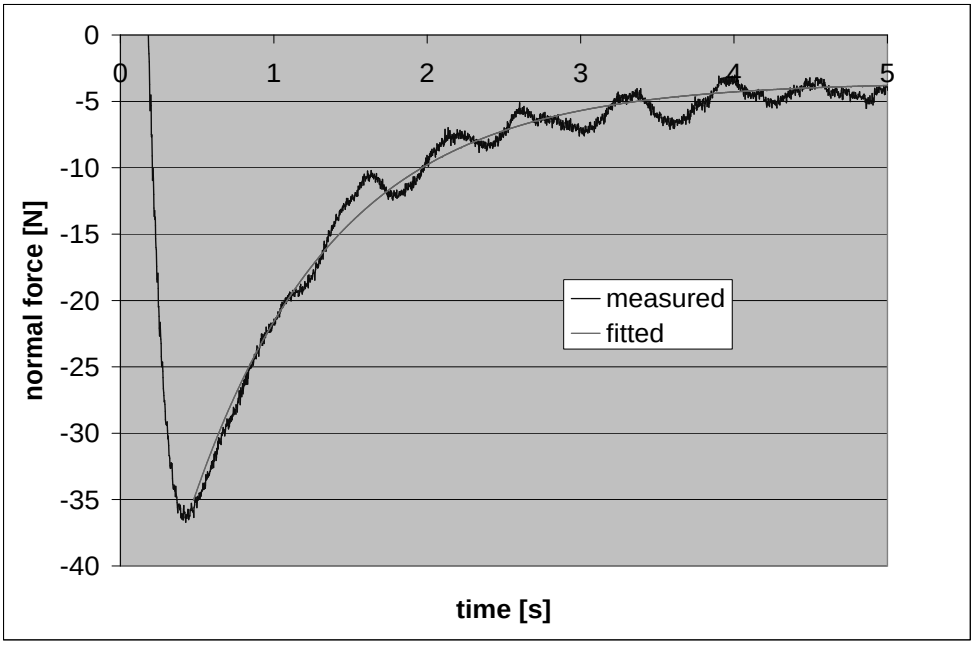


Figure 31: Normal force at 30% span (upward pitching step): Measured data and exponential data fit

# 8 Conclusions

The most important conclusions from the present study are:

- Dynamic inflow effects were clearly present in the NASA-Ames measurements at fast pitching steps;
- The upward pitching step is much more suitable for studying dynamic inflow effects than the downward pitching step. For the downward pitching step the angle of attack exceeds the stall angle of attack. The analysis of dynamic inflow effects is then complicated by the uncertainties which result from stall;
- The NREL measurements in the NASA-Ames tunnel allowed an assessment of the radial dependency on the dynamic inflow effect.
- The agreement between the measured results and the calculational results from the newly developed free wake lifting line model AWSM (for the upward pitching step) is excellent in terms of:
  - Equilibrium values of normal forces;
  - Overshoots in normal forces in reaction to the step in blade pitch angle
  - Time constants. These characterize the gradual approach of the normal forces towards the equilibrium values after the overshoot.
- The time constant in the measured and AWSM results, hardly reduces towards the tip. This is opposite to the results and theoretical expectations from earlier projects and from the engineering model for dynamic inflow as implemented in PHATAS.

## References


[1] A. van Garrel (2003): *"Development of a wind turbine aerodynamics simulation module"*. ECN-C –03-079, Energy Research Centre of the Netherlands, ECN.

[2] C. Lindenburg (2003): *"Investigation into rotor blade aerodynamics, Analysis of the stationary measurements of the UEA Phase IV rotor in the NASA-Ames wind tunnel"*. ECN-C –03-025, Energy Research Centre of the Netherlands, ECN.

[3] C. Lindenburg (2005): *"PHATAS, Release NOV-2003 and APR-2005 User's manual"*. ECN–I- 05-005, Energy Research Centre of the Netherlands, ECN.

[4] H. Snel (1997): *"Heuristic modelling of dynamic stall characteristics "*. Proceedings of the EWEC 1997 Conference held at Dublin. pages 429–433.

[5] H. Snel and J.G. Schepers (1994): *"JOULE1: Joint investigation of Dynamic Inflow Effects and Implementation of an Engineering Method"*. ECN-C-94-107, Energy Research Centre of the Netherlands, ECN.

[6] J.G. Schepers (2007): *"IEA Annex XX: Comparison between calculations and measurements on a wind turbine in the NASA-Ames wind tunnel"*. ECN-E-07-066, Energy Research Centre of the Netherlands, ECN.

[7] J.G. Schepers (2007): *"IEA Annex XX: Comparison between calculations and measurements on a wind turbine in yaw in the NASA-Ames wind tunnel. "*. E-07-072, ECN.

[8] J.G. Schepers and H. Snel (1995): *"JOULE2: Dynamic Inflow: Yawed Conditions and Partial Span Pitch"*. ECN-C-95-056, Energy Research Centre of the Netherlands, ECN.

[9] M.M. Hand et al (2001): *" Unsteady Aerodynamics Experiment Phase VI Wind Tunnel Test Configurations and Available Data Campaigns"*. NREL/TP- 500-29955, National Renewable Energy Laboratory, NREL.

[10] R. van Rooij (2005): *"The effect of the test set-up on the steady state aerodynamic data (IEA-Annex XX)"*. Proceedings of the IEA Aerodynamics Symposium held at CENER, Pamplona.

[11] T.G. van Engelen and E. van der Hooft (2004): *"Dynamic inflow compensation for pitch controlled windturbines"*. Proceedings EWEC conference, London, 22-25 November 2004 (on CD-ROM).